Experimentation of a Topology-Optimized Metal Structural Connection Under Casting Constraints

by

Andrew Novillo

B.Arch., The Pennsylvania State University, 2018

Submitted to the Department of Civil and Environmental Engineering in Partial Fulfillment
of the Requirements for the Degree of

Master of Engineering in Civil and Environmental Engineering

at the

Massachusetts Institute of Technology

June 2019

©2019 Andrew Novillo. All rights reserved.

The author hereby grants to MIT permission to reproduce and to distribute publicly paper
and electronic copies of this thesis document in whole or in part
in any medium now known or hereafter created.

Signature redacted

Signature of Author...
Department of Civil and Environmental Engineering
May 10, 2019

Signature redacted

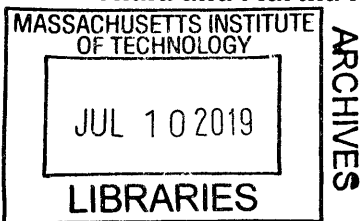Certified by ....
Josephine V. Carstensen
Lecturer, Department of Civil and Environmental Engineering
Thesis Supervisor

Signature redacted

Approved by..
Heidi Nepf
Donald and Martha Harleman Professor of Civil and Environmental Engineering
Chair, Graduate Program Committee

1

Experimentation of a Topology-Optimized Metal Structural Connection Under Casting Constraints

by

Andrew Novillo

Submitted to the Department of Civil and Environmental Engineering on May 10, 2019
in Partial Fulfillment of the Requirements for the Degree of
Master of Engineering in Civil and Environmental Engineering

Abstract

Topology optimization has only begun to emerge into the building industry because of the lack of testing being conducted to evaluate its performance. Within the civil engineering field, topology-optimized designs have to date mainly been produced as a proof of concept rather than for load testing. The hybridization of topology optimization and manufacturing presents an opportunity for the techniques to inform each other throughout the design process. This thesis proposes a study aiming to bridge the gap across disciplines by designing a topology-optimized building connection, finding an effective method to fabricate the design, and experimentally load-testing its behavior to verify the performance results.

A roof truss connection is chosen from the Scottish Parliament in Edinburgh, as it is a unique node joining eight elements from an unordinary truss. Abaqus with Tosca is then used to perform the topology optimization. An elastic continuum design is set up using the Tosca engine with a density-based approach. The specified objective for the test is minimization of the global compliance, which corresponds to a maximized stiffness of the connection, subject to a varying volume constraint and casting constraints.

The connections are then investment cast out of aluminum in the MIT foundry. The conventional casting process incorporates 3D printing to help create the free-form geometries of the optimization. The complex load case of the connection requires a custom testing frame to be built to simulate the roof truss.

There are many challenges associated with testing physical specimens in the field of structural engineering. In this work, it was found that the casted material contains imperfections that affects the experimentation results. While the experimental results are not directly comparable to the numerical predictions, the specimens themselves are comparable. The original connection appeared as the strongest specimen in the experimentation for ultimate loads, had the highest stiffness, and lowest compliance.

This experiment shows how sensitive optimization is to material properties, boundary conditions, casting process, and volume constraints. This study provides the framework for creating an optimized connection that performs the same in physical experimentation as it does computationally.

Thesis Supervisor: Josephine V. Carstensen
Title: Lecturer, Department of Civil and Environmental Engineering

3

Acknowledgements

First of all, I would l like to thank my family, friends, and especially my parents for their continued support to follow my dreams and ambitious aspirations, no matter what they are. My parents help me to overcome life's many obstacles so that I may continue to focus on my work and do what I enjoy. Without them, MIT would not have been possible.

I would like to express my deep appreciation for Josephine Carstensen, who has been more than a thesis advisor for this project. She is a teacher, an advisor, and an all-around supporter for all of the ideas and lessons I've learned throughout this year. Her patience, motivation, and creativity has made this thesis possible. She continuously took time out of her day to make sure I had a thorough understanding of the topology optimization material required for this thesis, and for that I am grateful.

I would like to thank Michael Tarkanian who helped to make investment casting possible. Even when I was told by others that my project was unfeasible, he stood up to the challenge. His guidance and advice for teaching me casting allowed this thesis to be completed.

I would like to extend sincere thanks to Stephen Rudolph for helping to create the experimental load testing frame. He took the time to figure out and model the entire assembly needed for the testing frame to be completed. More than that, he taught me many different tools and techniques in the machine shop that I am grateful for. Even though he had many students' project to balance, we managed to finish the testing setup in an efficient time frame. He also quickly handled all of the unexpected problems that this thesis presented.

I would like to thank Arup and Tali Mejicovsky for permitting me to use their drawings of the Scottish Parliament Roof Truss Connection.

I would like to thank José Duarte of Penn State University, as he saw the potential in me and encouraged me to apply to MIT while completing my B. Arch degree.

I would like to thank all of my fellow MEng colleagues; together we figured out and learned an extraordinary amount of material during this intense year. The different perspectives and feedback they provided me with allowed me to see my thesis in ways I had not thought of before.

To my significant other, Marlene Sharp, her support, intelligence, and strive for hard work has continuously motivated me throughout my graduate education. I am extremely thankful for her help editing and proofreading, listening to my rants, and pushing me to complete this thesis.

I would like to thank additional professors of the MEng program, Gordana Herning and Caitlin Mueller, for their advice and support throughout my thesis.

I am truly grateful for my opportunity to study at MIT, whose educational philosophy of "Mind and Hand" are practiced throughout this thesis. At this institution, I was finally able to pursue all of my diverse academic interests without being constrained by my major.

Thanks to you as well, the reader, for taking the time to read this. May this thesis stir your imagination, generate creative ideas, and inspire you to pursue your goals the same way it did for me.

Table of Contents

List of Figures

List of Tables

Introduction

1.1 Overview and Motivation

Figure 1 Cantilever Beam (Galilei 1638)
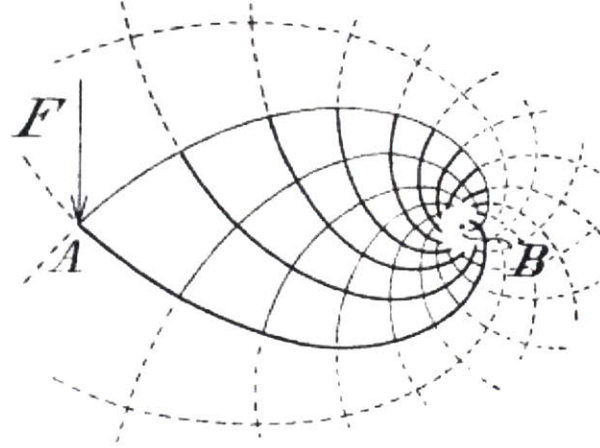
Figure 2 Optimized Truss (Michell 1904)

Beam design and optimization began as theories introduced by Galileo, as shown in **Figure 1** (Galilei 1638), which grew over time into a mathematical derivation of a Michell truss, as shown in **Figure 2** (Michell 1904). Today, optimization has evolved into a new generation of topology optimization software tools developed in recent decades. This process allows for the creation of high-performance structures through an efficient placement of material (Bendsoe and Sigmund 2004). Topology optimization takes a normal structure (load, design space, boundary conditions) and applies an iterative algorithm that works towards an objective following certain constraints. Objectives may, for example, include stiffness (or compliance), minimum mass, and maximum displacement. Constraints may include the percentage of mass removed, maximum deflection, and minimum thickness of the structure. The iterations may be conducted with a genetic algorithm, which strategically tests many different possible samples of the design space, or a gradient-based algorithm that chooses a starting point and methodically moves towards convergence. This study used a gradient-based algorithm. (Chaparro et al. 2008) may be referred to for more information on how different optimization algorithms affect the resulting design.

There are still many issues present with topology optimization, such as complex final designs and the extensive amount of time required to explore all of the design possibilities.

Additionally, numerical instabilities such as mesh-dependence and checkerboards are well-established (O. Sigmund and Petersson 1998). However, these can be resolved by applying a filter to a mesh element to account for its surrounding elements. Some examples include the sensitivity filter to modify the real sensitivities with the sensitivities of the surrounding elements (Ole Sigmund 1994), the density filter (Bruns and Tortorelli 2001), and the Heaviside Projection Method (Guest, Prévost, and Belytschko 2004).
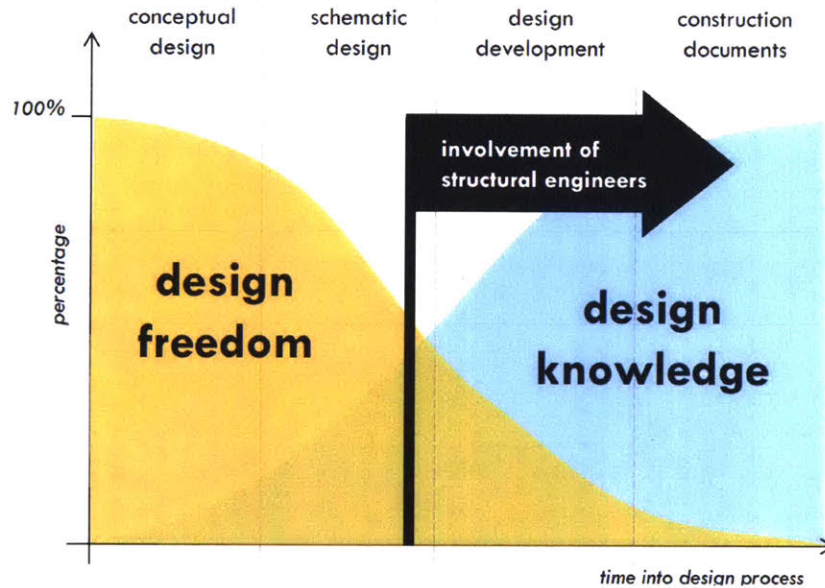
Figure 3 Relationship between design freedom and design knowledge in building design projects (Mueller and Ochsendorf 2013)

Topology optimization has been used for design purposes in many fields such as the automotive industry, mechanical engineering, and aerospace engineering. However, there are a limited number of examples of the application of topology optimization for the design of civil engineering structures. This is due to the abundance of codes and safety requirements, as well as the non-standardization of building components in buildings. Mueller and Ochsendorf argue that the best time to implement optimization is early on in the design process while the greatest amount of opportunity for exploration is still available, as shown in **Figure 3** (Mueller and Ochsendorf 2013). This would suggest that optimization may exist at the conceptual level to help develop an initial geometry and form for a building, as done by (Stromberg et al. 2011) shown in **Figure 5**. Other examples of the application of optimization exist at a more practical level; for example, it may be utilized for an efficient layout of rooms or a repositioning of the structural grid (Michalek, Choudhary, and

Papalambros 2002). Further studies have been performed on component scale applications, such as optimizing strut-and-tie models in concrete beams, as shown in **Figure 4** (Bruggi 2009). This study focuses on a more detailed, small-scale component in buildings: structural connections.
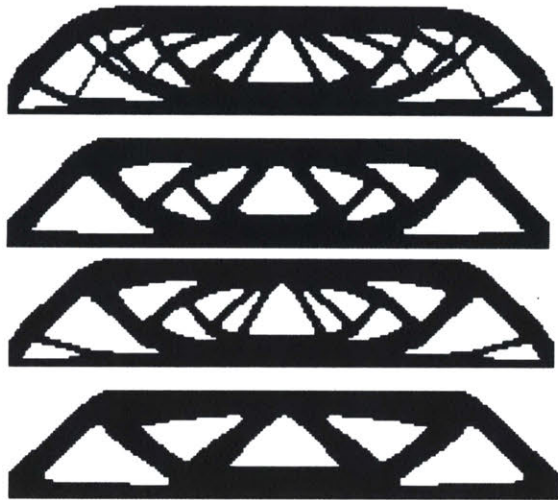
Figure 4 Optimized Strut-and-Tie Layouts for Concrete Beams (Bruggi 2009)
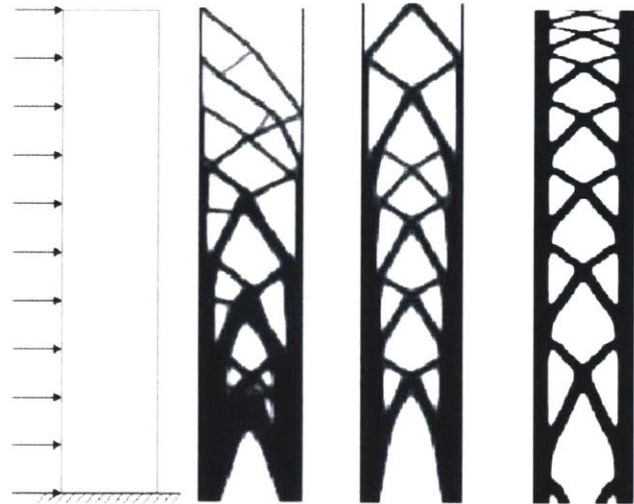
Figure 5 Optimized cantilever example used for conceptual structural design of a high-rise building (Stromberg et al. 2011)

There is an abundance of complex connections that may take place in a construction project requiring a multi-part assembly. These multifaceted connections may exist in the building industry through facade connections and trusses. There are three types of structural connections defined in buildings: internal, external, and splices (Boake 2015). Internal connections are the individual parts of an assembly which help to construct a whole external connection. External connections are the pieces that link all of the other elements such as beams, cables, and columns together in a building. For larger projects, a member may sometimes be too large for transportation and may require being split up into smaller pieces. This instance would call for a splice connection, which links two or more parts of a continuous element. This study focuses on an external connection, linking four beams and four cables together into a single node.

Manufacturing technologies have developed significantly over recent years and may exist as a subtractive or additive method; this paper focuses on the latter. The additive manufacturing of metal parts allows for the connection to be fabricated in a single pass while still achieving the required structural strength (Gibson, Rosen, and Stucker 2015). Common

13

forms of additive manufacturing in the industry are 3D printing and casting. While 3D printing is newer than casting, it has found industrial use through the automotive, mechanical, and aerospace industries. Examples include an aircraft engine bracket by GE (Carter et al. 2014), a car's brake caliper by Bugatti (Molsheim and Wolfsburg 2018), and passive coolers for light-emitting diode lamps (Alexandersen, Sigmund, and Aage 2015).

No examples of built structures with 3D-printed connections presently exist. However, rather than 3D printing the connection itself, 3D printing may be used to modify the casting process. Casting is limited to what may be assembled into a mold, and 3D printing is limited by the size and amount of material. Instead of 3D printing the structural connection itself, 3D printing can be used as a part of the process to manufacture an organic, geometrical mold for casting liquid metal (Gatto et al. 2007).

The hybridization of topology optimization and manufacturing presents an opportunity for the techniques to inform each other throughout the design process. Topology optimization has only begun to make its way into the building industry because of the lack of testing being conducted to evaluate its performance. This study utilized an available commercial software, Abaqus with Tosca ("Abaqus Analysis User's Guide" 2014), to design and evaluate a structural connection under a complex loading scenario. To verify the results from the digital model, the connections were fabricated using investment casting aided by 3D printing to assemble the mold. Experimentation was then conducted to analyze the strength performance versus the material savings of the optimized connections.

1.2 Literature Review

The following literature review is broken up into three sections. The first section discusses precedents of optimized connections, and how they were applied both within and outside of the civil engineering discipline. The second section discusses different softwares available for implementing topology optimization, why Tosca was chosen, and the different iterative algorithm functions that may be used for optimization. Finally, the third section discusses the benefits and drawbacks of investment and sand casting, and why investment casting was chosen for the basis of this study.

1.2.1 Optimized Connections Precedents
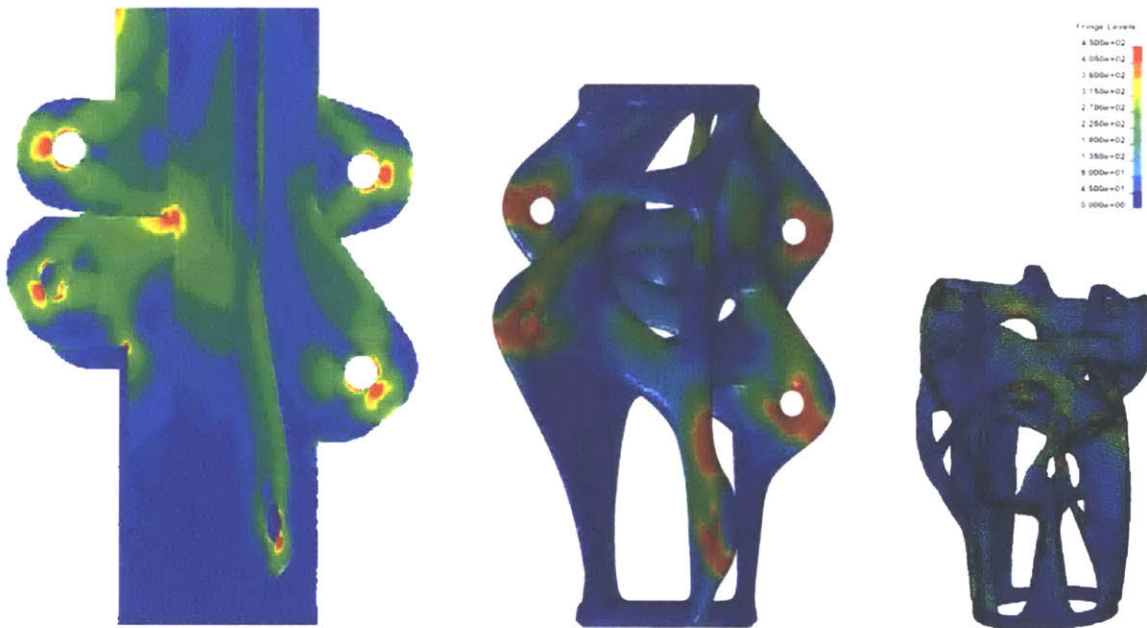
Figure 6 Von Mises Stresses of Optimized Connection (Galjaard et al. 2015)

For the connection design of civil structures, design firms such as ARUP and Simpson Gumpertz & Heger Inc. have begun to integrate topology optimization for real-world building applications. Arup conducted a conceptual study for an art tensegrity structure at Grote Marktstraat in The Hague, Netherlands, as shown in **Figure 6** (Galjaard et al. 2015). The study optimized a connection which linked cables and struts to a lighting fixture, while also allowing adjustability of the cable's length. The design objective was to minimize the total structural weight. Altair's Optistruct (*OptiStruct* 2019) was used to achieve a connection with a 50% weight reduction, leading to both compression in the strut and tension in the

cables being reduced by 20%. The part was fabricated; however, the part was designed after the projected was completed and never installed or load tested.

The fabrication of the part was completed through Direct Metal Laser Sintering (DMLS). This process involved layers of metal powder being laid onto a bed, while progressively being laser melted in certain areas in order to form the geometry of the part. This form of 3D printing metal was the most feasible fabrication method for the specific geometry, as creating a casting mold with inner voids was deemed difficult. Because of the complex geometry, the original node was redesigned to link the cables using a bolt as a 'stopper and a spanner' instead of the original pin & fork connection.
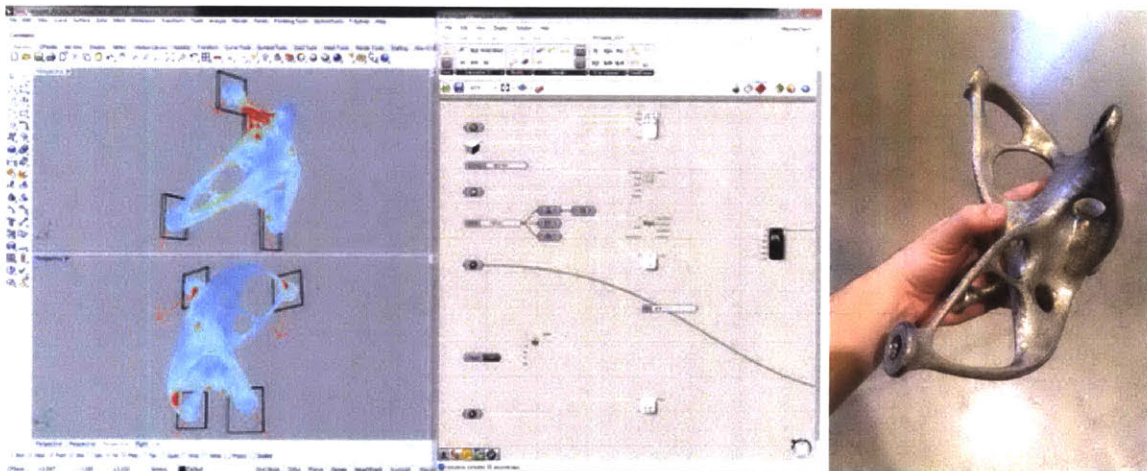
Figure 7 Wind forces on Optimized Model (Menges et al. 2017)

Simpson Gumpertz & Heger Inc. (SGH) also explored the benefits of optimization in the building industry by using mass customization, reduction of assembly effort, and the production of forms not possible before (Menges et al. 2017). The work focused on a structural project for the entrance building in Northern MA. The project contained unique façade connectors between a glass panel and the slab edge with many varying distances. SGH developed custom C# scripts within Grasshopper/Millipede using the building façade geometry as the input, as shown in **Figure 7**. The generated geometry was then exported to ANSYS8, and a multi-objective topology optimization was performed as well as a detailed finite element analysis. The geometry was then imported into ZBrush9 in order to smooth the surface profile and clean up the mesh. Finally, the part was imported back into ANSYS for re-analysis and a final sign-off against load capacity criteria. The way this optimization was conducted involved multiple conversions between programs in order to assemble the

16

geometry, optimize it, and then analyze it. As with most digital conversions, there was likely data lost in translation between the programs. The workflow may have been improved by involving fewer programs in the process, thus creating a more seamless transition between optimization and analysis.

In order to ensure the part was capable of being fabricated, SGH worked with Addaero Inc. (*Addaero* 2016) of New Britain, Connecticut. Addaero provided advice on printing constraints, such as maximum size, local thicknesses, and the accuracy needed from the geometry file. The final printed connector was hollowed out with a shell thickness of 1.5mm "optimized for architectural and structural performance" (Menges et al. 2017). This was most likely done because of the expensive cost associated with 3D printing a fully solid metal part. While the part was successfully fabricated, no load testing was completed to determine if the optimized part met its performance requirements, or if hollowing it out affected its structural integrity.

Beyond the civil engineering industry, topology optimization is popular for design within the automotive and aerospace industries, as low weight is important for fuel consumption and parts are mass-produced. Not only are these parts being designed, but they are also being tested for application in real-life scenarios. Within the aerospace industry, optimization may be applied to "standard material layout design for airframe structures, layout design of stiffener ribs for aircraft panels, multi-component layout design for aerospace structural systems, and multi-fasteners design for assembled aircraft structures" (Zhu, Zhang, and Xia 2016). Within the automotive industry, Bugatti has designed the world's first optimized brake caliper to be fabricated by a 3D printer for one of their cars. (Molsheim and Wolfsburg 2018).

GE recently held a challenge to find mechanical design concepts for an aircraft engine bracket (Carter et al. 2014). Because this bracket was so commonly used within airplane engines, it was calculated that all the aircraft in the world could have a savings of $5M - $9.5M per year, which equates to around 1.7M-3M gallons of jet fuel. This demonstrates that the optimization of a simple bracket may not only be beneficial from a business perspective, but also from an environmental perspective. Designs were critiqued not only by their expected

performance and material savings, but also through their ability to be properly fabricated and accurately load-tested.
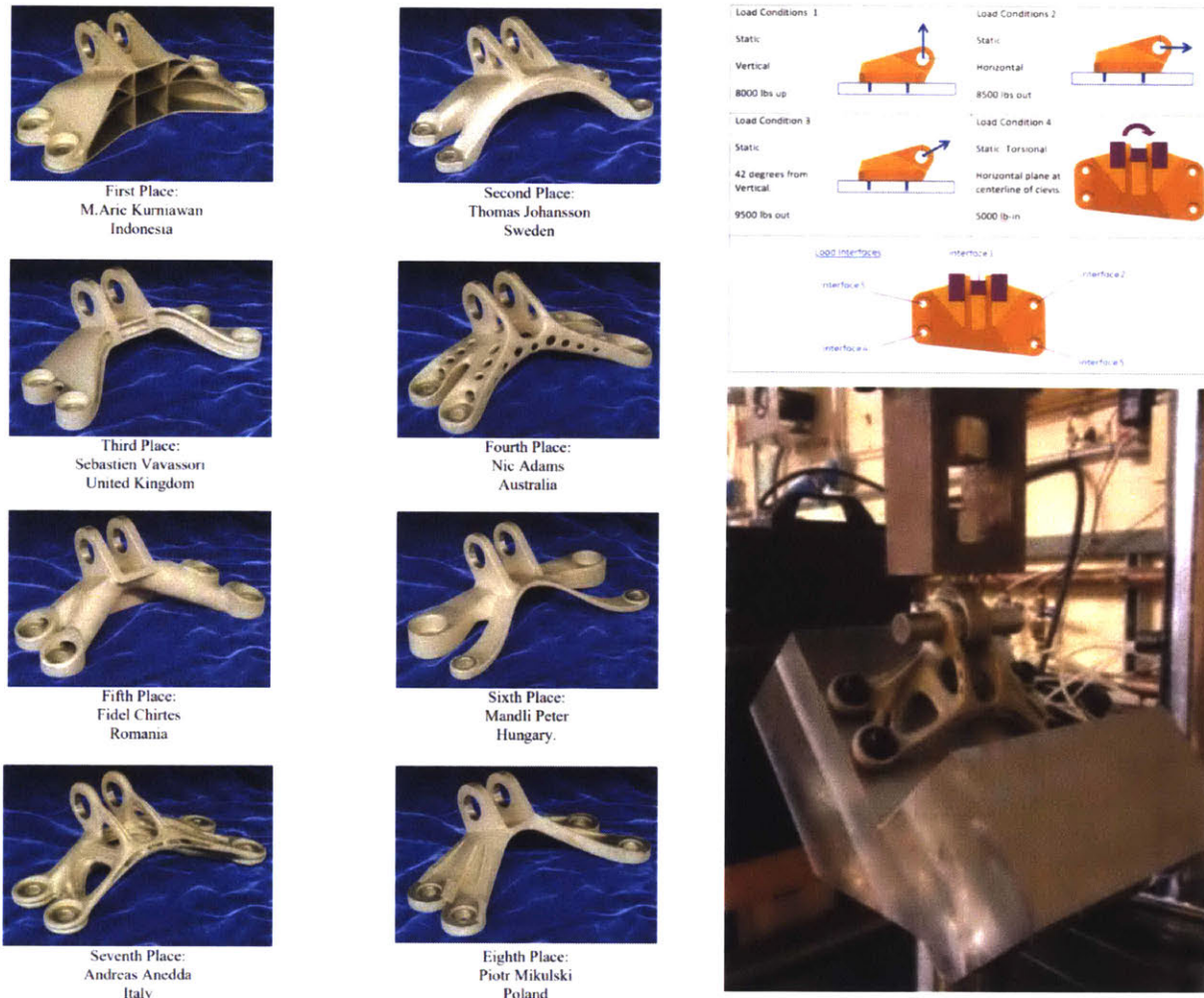
Figure 8 Winning Bracket Designs & Load Conditions & Load Testing (Carter et al. 2014)

In this study, GE was able to filter out the initial entries by ranking them based on volume and running a FE analysis to ensure none of the part exceeded the yield stress of the base material. The parts were then 3D printed out in titanium. As shown in **Figure 8**, each part was loaded into a custom testing rig to examine if the performance was comparable to the FE analysis results and if it met all of the loading conditions. The best design was able to fully support the design loads while attaining only 20% of the original bracket's weight. As compared to the original design, the winning bracket would save 3.76lbs, resulting in fuel savings from 12M to 22M gallons of jet fuel, equating to $37M - $71M, higher than originally estimated.

Bugatti worked on designing a new brake caliper for the new Chiron, one of the fastest production cars in the world (Molsheim and Wolfsburg 2018). Weight was a significant factor when it came to breaking the top speed record, and this optimized design was able to reduce the weight by 40%; from 4.9 kg to 2.9kg. Creating a car part of this precision could only be done with laser powder-bed fusion (LPBF), an alternate form of 3D printing metal. A titanium alloy was used for fabrication.

Figure 9 Bugatti Brake Caliper with Pistons and Pads Fabricated & Tested (Molsheim and Wolfsburg 2018)

It took 45 hours to print the brake caliper and 11 hours of post-processing in a five-axis milling machine to create the contact surfaces and threads. Surprisingly, the piece was not solid; it was instead hollow. For more information on why the piece was hollow, (Ole Sigmund, Aage, and Andreassen 2016) may be referred to. The piece was fabricated with a wall thickness ranging from one to four millimeters. The design was put to the test at speeds that the Chiron can achieve, as shown in **Figure 9**. Near the top speed at 375 km/h (233mp/h), the brake was fully applied to simulate bringing the car to a complete stop (Volkswagen Group 2018). This was reiterated to ensure the caliper could handle the stresses and temperatures needed, reaching temperatures up to 735 °C (1355 °F).

As the above examples illustrate, optimized connections exist across different engineering disciplines; however, there is a noticeable difference in the frequency of their application. In the aerospace and automotive industries, designs are fabricated, analyzed, and put to the test to verify that material may be saved without compromising performance. Within the civil engineering field, designs have to date mainly been produced as a proof of concept rather than for load testing. This study aims to bridge the gap across disciplines by designing a topology-optimized building connection, finding an effective method to fabricate the design, and experimentally load-test its behavior to verify the performance results.

1.2.2 Topology Optimization Software

SELECTION OF TOPOLOGY OPTIMIZATION SOFTWARE

INTEGRATED ON MULTIOBJECTIVE OPTIMIZATION

- OPTISTRUCT (ALTAIR)
- GTAM (ANSYS)
- TOSCA (DESSAULT SYSTEMS)
- ATOM (DESSAULT SYSTEMS)
- BESO 3D (DESSAULT SYSTEMS)
- GENESIS (VR&D)
- FEMAP/NX NASTRAN (SIEMENS)
- LS.OPT/LSOPT
- FEMTOOLS OPTIMIZATION (DINAMIC DESIGN SOLUTIONS)
- MILLIPEDE (GRASSHOPPER)
- TOPTOP (GRASSHOPPER)

FREE LICENCE SOFTWARE AND SUPPORTING DOCUMENTATION

- OPTISTRUCT (ALTAIR)
- GTAM (ANSYS)
- FEMAP/NX NASTRAN (SIEMENS)
- MILLIPEDE (GRASSHOPPER)
- TOPTOP 2D AND 3D (GRASSHOPPER)

Figure 10 Topology Optimization Software (García-Domínguez, Claver, and Sebastián 2017)

There exists several commercial softwares used in the building industry to perform topology optimization. Garcia-Dominguez et al. discusses in-depth the differences between structural optimization softwares when accounting for 3D printing constraints (García-Domínguez, Claver, and Sebastián 2017). **Figure 10** lists all of the software available in 2017. This work utilized the commercial software, Abaqus, to conduct the FE analysis, with Tosca used to conduct the topology optimization. Tosca may be used to help find the ideal distribution of material within a set design space in order to meet a defined objective function under certain constraints ("Abaqus Analysis User's Guide" 2014).

The process in which the optimization is conducted in Abaqus with Tosca is shown in **Figure 11**. Tosca uses one of two available algorithms for topology optimization: a sensitivity-based solver or a controller-based solver. The controller-based solver is limited to using compliance as the objective function and using volume as a constraint, while using strain energy and grid point stresses for the optimization. The major advantage of using a controller-based solver is that it is much faster than the sensitivity-based solver. This study used the sensitivity-based solver of Tosca, a general algorithm partly described in (Bendsoe and Sigmund 2004). This method allowed for a more accurate solution along with more possibilities for the objective functions and constraints of the optimization.
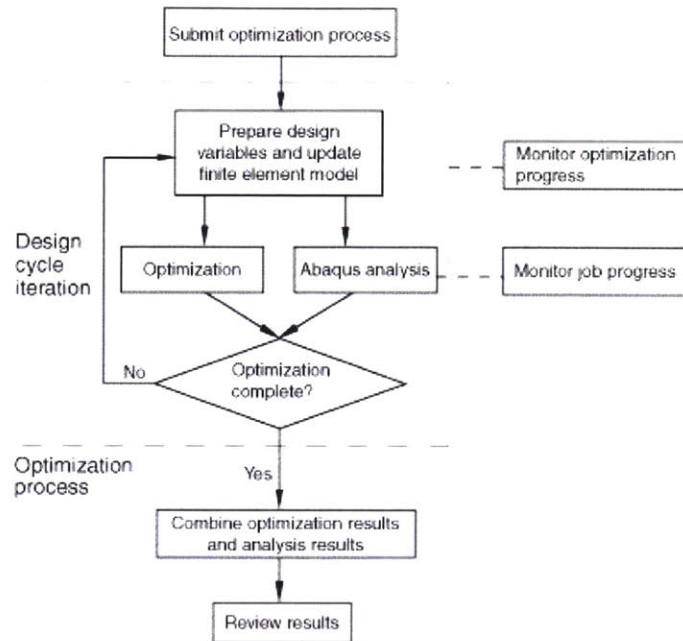
Figure 11 Tosca Optimization Process - General ("Abaqus Analysis User's Guide" 2014)

1.2.3 Investment vs. Sand Casting Process

Investment and sand casting are both processes used to create metal parts by pouring liquid metal into a three-dimensional mold. Both are similar in terms of fabrication process, but vary in terms of resulting precision, cost, time, and skill level (Done 2016). The process starts with an initial positive, which is ideally made out of wax, as that is the easiest and cleanest to remove. Any other material that is able to be burned out of a mold may also be used; some of these other materials include wood, plastic, or organic materials.

Next, the negative mold must be made. Through investment casting, the mold is formed by dipping the wax into a liquid ceramic slurry, which then hardens as it dries. With sand casting, sand is compacted in two separate halves around the positive, which are then

COMPARING SAND AND INVESTMENT CASTING		
	Investment Casting	Sand Casting
Relative cost in high quantities	Low	High
Relative cost for small quantities	Low	Medium
Weight limit of casting	<700 lb	<2,000 lb
Thinnest possible wall (in.)	0.0625	0.1
Dimensional tolerance (in.)	0.01	0.12
Surface finish	Very good	Fair to good
Ease of casting complex design	Excellent	Fair to good
Ease of changing design	Fair	Excellent

Figure 12 Investment vs. Sand Casting Performance Comparison (Done 2016)

tied together to form the complete mold. After sprues and vents are added to the mold, it is ready for metal pouring. The final metal parts often have to be broken out of the molds, for both casting types, which prevents their reuse for multiple copies of the part.

There are several differences between investment and sand casting (Done 2016) as shown in **Figure 12**. The first difference is that this study's connections contained complex geometries that were not separable into two half molds. Therefore, sand casting could not be used for the scope of this thesis. Investment casting is a more precise fabrication method, which is necessary for the connections in this work. There is very precise detail in investment casting, along with consistency between the molds. Furthermore, it would be difficult to control the molds with sand casting, as the compaction is done by hand.

Physical Properties	Metric	English
Density	2.67 g/cc	0.0965 lb/in³
Mechanical Properties	**Metric**	**English**
Tensile Strength, Ultimate	>= 234 MPa	>= 34000 psi
Tensile Strength, Yield	>= 165 MPa @Strain 0.200 %	>= 24000 psi @Strain 0.200 %
Elongation at Break	>= 3.5 %	>= 3.5 %
Modulus of Elasticity	72.4 GPa	10500 ksi
Poissons Ratio	0.33	0.33
Machinability	50 %	50 %
Shear Modulus	27.2 GPa	3950 ksi
Shear Strength	143 MPa	20700 psi

Figure 13 Aluminum A356-T6 Properties (Matweb)

Investment casting was chosen moving forward to create these parts; its limitations were addressed as constraints within the topology optimization software. The weight limit of casting at the MIT foundry was 30lbs., which allowed for multiple parts to be cast simultaneously. A test cast was initially performed, which made it clear that a minimum thickness of 0.125" should be allowed anywhere throughout the parts. The metal used for structural parts was the aluminum alloy, A356. The physical and mechanical properties of A356 are included in **Figure 13** ("Aluminum A356.0-T6, Sand Cast" 2019). The most important properties necessary for this work are the density, modulus of elasticity, Poisson's ratio, and yield strength.

Methodology

2.1 The Scottish Parliament Connection
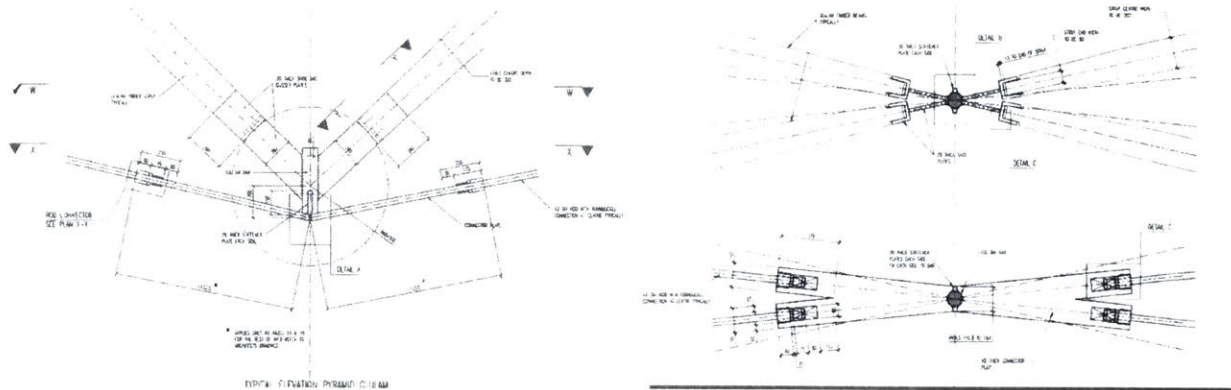
Figure 14 Scottish Parliament Roof Truss Connection Construction Drawings – ARUP

The Scottish Parliament was designed by Enric Miralles and opened in 2004 as one of the most innovative designs in the United Kingdom. It is located in Edinburgh and was built from a variety of materials, such as steel, oak, and granite ("About The Building" 2014). **Figure 14** shows the construction drawings used for the Scottish Parliament Roof Truss Connection, provided directly by ARUP for educational purposes. A roof truss connection was chosen as it was a unique node joining eight elements (four in compression and four in tension) in an unordinary truss. The connection was simple enough to be symmetrical both in the x-axis any y-axis, but complex in its angularity in both planes. Not only does the connection perform well structurally, but it was also highlighted architecturally throughout the debating chamber. An interpreted Rhino model was produced at 1" = 1'-0" scale as close to the original dimensions as possible. This scale was chosen by the constraints of the investment casting process used in this study.
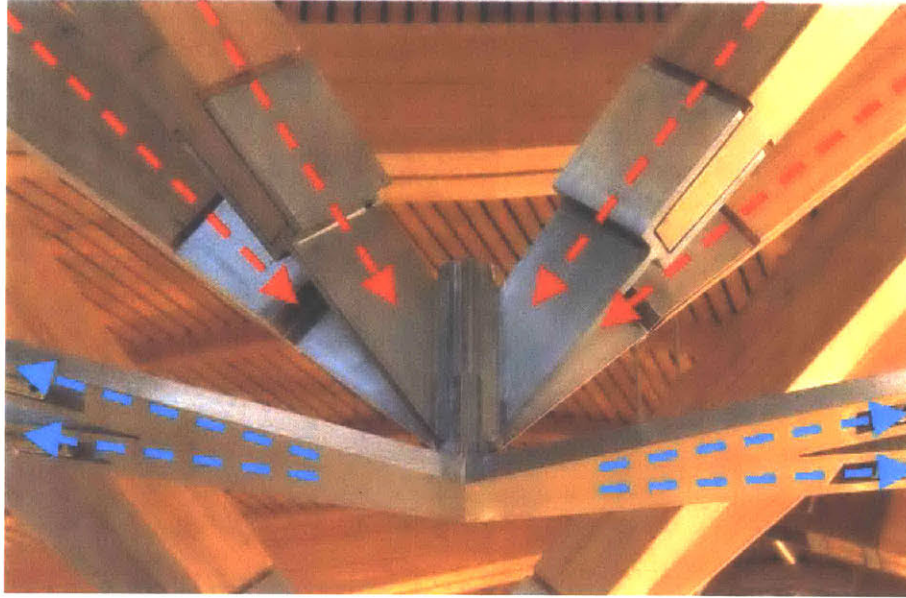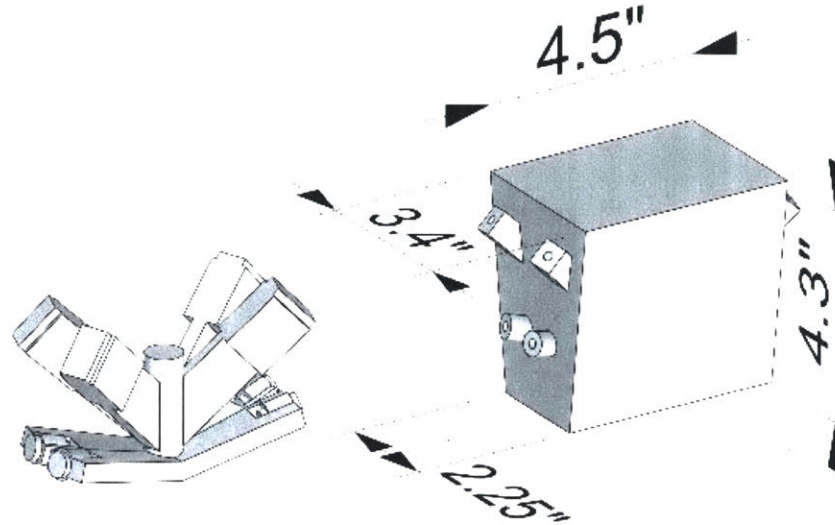
Figure 15 Scottish Parliament Connection Forces

As for any structure, it is important to understand the flow of forces within the connection. As shown in **Figure 15**, the four wooden elements shown with red arrows represent compression forces from the roof loads being transferred onto the connection, creating the resultant four tensile forces in the steel rods shown in blue. These tension and compression forces do not act in the same plane, and can be more clearly read in plan on the construction drawings provided by ARUP in **Figure 14**. This study wishes to redesign this truss connection using topology optimization to evaluate if its performance can be improved with a more efficient layout of material.

2.2 Topology-Optimized Connection Design

2.2.1 Rhinoceros 3D (Rhino) Digital Modelling

Figure 16 Original Connection & Optimization Dimensions

The next phase of redesigning the Scottish parliament connection with topology optimization involved digital modeling. Most of the digital modelling was performed in Rhino rather than in Abaqus, as it was more efficient to model complex geometry and details in Rhino, with its wide range of commands available for use. In **Figure 16**, the original connection was created in Rhino on the left, and the design space and boundary conditions were modeled with dimensions shown for the optimization on the right. Taking into consideration the experimentation of the testing setup, the connection had rods screwed directly into it in order to apply the forces and create the reactions. This condition was also modeled into the part's boundary conditions where the loads and supports would be applied.

The design space was offset to be greater than the original connection's dimensions to allow the optimization to assign material wherever it needed to outside of the original domain. **Figure 17** shows that the initial design space in 'Version 1' was too large, resulting an inefficient use of computational time to run the optimization. 'Version 2' was contrary to 'Version 1', as it was too small and limited where material could be placed. After performing several test optimizations with a coarse mesh, the final trapezoidal design space in 'Version 3' was modelled just large enough so that it would not limit the algorithm, but also small enough to run the iterations in a timely manner.

25
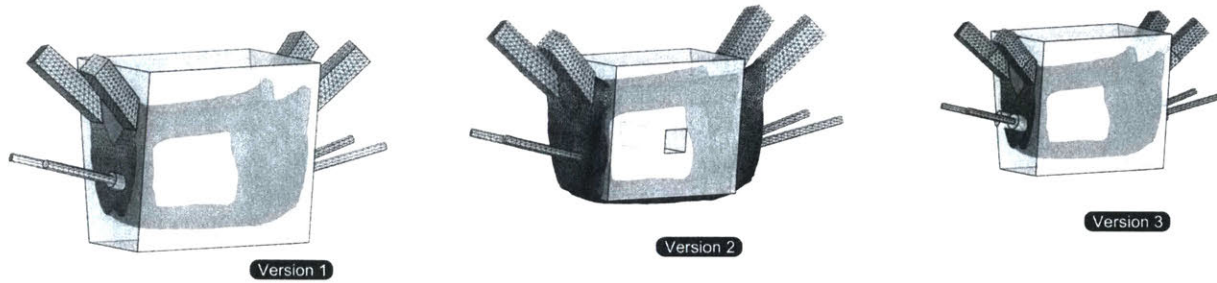
Figure 17 Design Space Adjustment

It was critical that the 3D geometry was clean and formed a completely closed poly-surface. To better streamline the transition from Rhino to Abaqus, it was more efficient to join all of the surfaces in Rhino and then partition them later in Abaqus, rather than export all of the parts separately and create an assembly within Abaqus. The most effective format to export the geometry cleanly into Abaqus was as a .stp file. This allowed meshing to be done through Abaqus, which helped to minimize translation errors between the two programs.

### 2.2.2 Abaqus & Tosca Topology Optimization
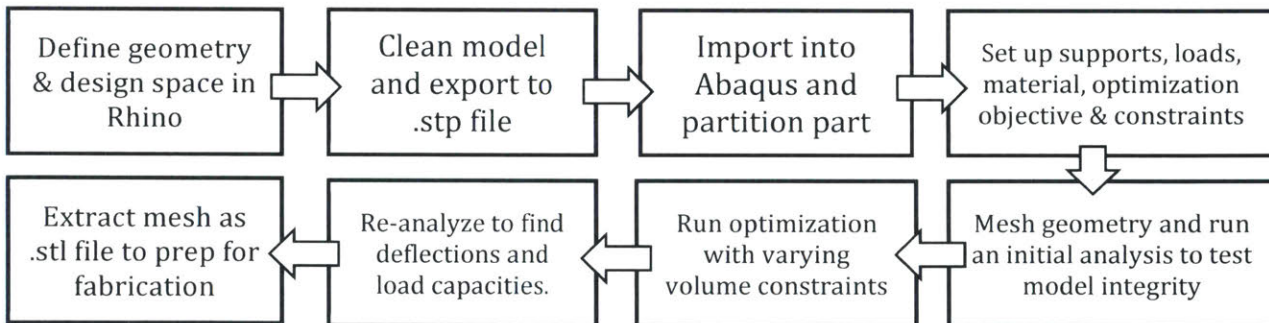
Figure 18 Optimization Workflow

Abaqus was chosen as the commercial software, since it provides a built-in finite element analysis (FEA) software as well as Tosca for the topology optimization ("Abaqus Analysis User's Guide" 2014). The digital work flow between programs is presented in **Figure 18**. After importing the geometry into Abaqus as a single part, the design space was partitioned separately from the boundary conditions. While the entire part contained the same material, different section properties were assigned to the part so that the optimization knew what the controls and variables were. As shown in **Figure 19**, the design space is represented in dark gray while the boundary and loading conditions are shown in white. The

loads shown in purple were applied to the face of the drilled hole to closely represent the experimental test set-up. The applied load was 1 kip, but the value of the load was not critical to the optimization as long as linear elasticity was assumed. Because of the way that the load testing was setup, all of the horizontal forces and reactions should have resolved within the connection, resulting only in a vertical force downwards. As the tension rods were screwed into the bottom of the connection, they were expected to rotate symmetrically at the connecting face of all four rods, shown in orange, creating the downward displacement. This rotation defined the boundary conditions as pinned supports.
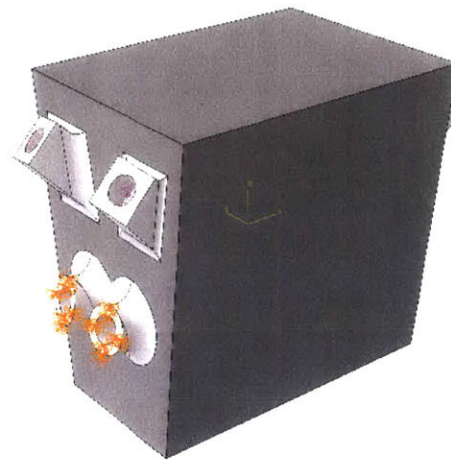
**Figure 19** Abaqus Boundary Conditions

Setting up the material in Abaqus involved using the properties from the A356 Aluminum specifications sheet ("Aluminum A356.0-T6, Sand Cast" 2019). The most notable properties are represented in **Table 1**.

Properties	Values
Density	0.0965 lb/in^3
Yield Strength	24000 psi
Poisson's Ratio	0.33
Modulus of Elasticity	10500 ksi

Table 1 Material Properties for Optimization

A continuum optimization was then set up using the Tosca engine with a density-based approach. This approach begins with a mesh of varying element size depending on

27

how detailed of a design solution is required. Each finite element (FE) of the mesh is then assigned a density varying between 0 (void) and 1 (solid). The elements are iteratively reassigned a density to determine the most efficient layout of material. An example of a simply supported beam, with a point load, being optimized using the density-based approach is shown in **Figure 20**. For more information on the density based approach to topology optimization, Bendsøe and Sigmund may be referenced (Bendsoe and Sigmund 2004).
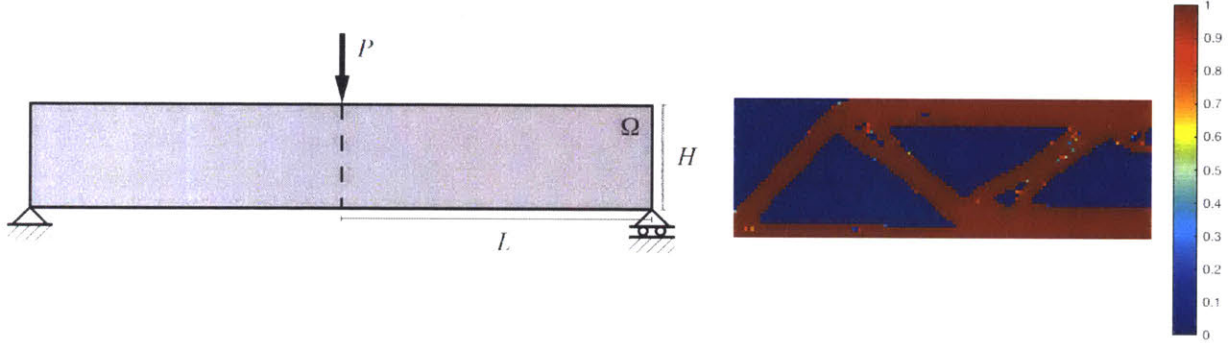
Figure 20 Beam Density-Based Optimization Example

In this study, the objective was to minimize the global compliance, which then maximized the stiffness of the connection subject to a varying volume constraint. The complete design problem was set up as follows:

$$\underset{\rho^e}{\text{minimize}} \quad f = \mathbf{F^T d}$$

$$\text{subject to} \quad \mathbf{h} = \mathbf{K}(\rho^e)\mathbf{d} - \mathbf{F} = 0$$

$$g = \sum_{e \in \Omega} \rho^e v^e - V \leq 0$$

$$\rho^e_{min} \leq \rho^e \leq 1 \quad \forall\, e$$

Equation 1 Optimization Function

Here ρ^e is the element density for element e, v^e is the element volume, V is the allowable material volume, and ρ^e_{min} is a small positive number to maintain positive definiteness of the global stiffness matrix. In addition, $\mathbf{K}(\rho^e)$ is the global stiffness matrix, $\mathbf{F}$ is the global load vector and $\mathbf{d}$ contains the free displacements. The stopping tolerance was taken as $\varepsilon = 0.001$ and the minimum density, $\rho^e_{min,}$ as 10^{-4}. The volume constraint was defined as 20%, 10%, and 7.5% of the dark gray design space volume. A geometric restriction of 0.125" minimum thickness was applied in order to consider casting tolerances.

28

The way in which Abaqus interacts with the design function and handles the optimization process is shown in **Figure 21**. The topology optimization starts with an initial design that is turned into a mesh with an even density for the elements. Then an analysis simulation, complete with loads, constraints and boundary conditions, is conducted. The optimization process redistributes the material at each iteration by changing the density of the elements in the design mesh while making sure to satisfy the optimization constraints ("Abaqus Analysis User's Guide" 2014). How the optimization process knows to redistribute the elements' densities is based on a sensitivity analysis at each iteration, which provides the derivatives of the design objective with respect to the constraints. The sensitivities then instruct the algorithm in both the step direction and size to take for the next iteration. This process is then iterated until the minimum compliance is reached based on the stopping tolerance following the given constraints.
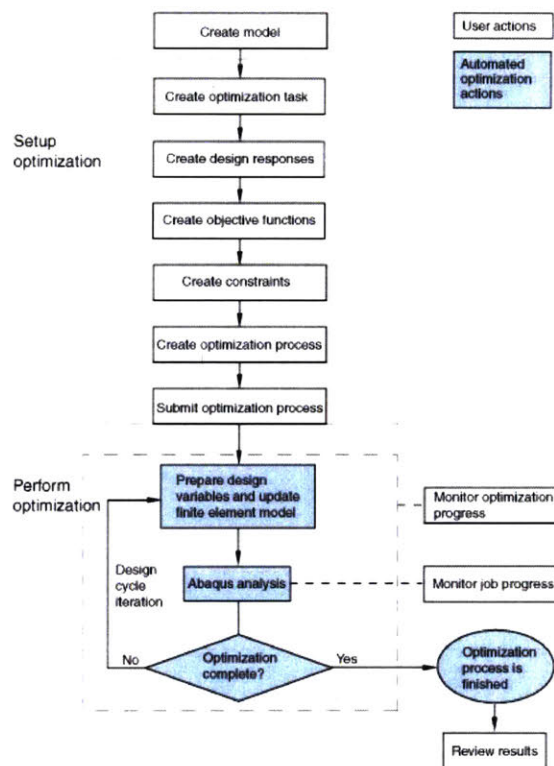
Figure 21 Tosca Optimization Process - Detailed ("Abaqus Analysis User's Guide" 2014)

The aim of the optimization is to produce solid and void material; however, fictitious material of a density in between 0 and 1 is allowed as the optimization progresses. Despite this allowance, it is more accurate to have a binary solution that leaves only void and solid material to create a more realistic structure.0 As discussed by (Jewett 2018), there is no

longer a necessity for post processing, which may have an undesirable effect on the final design. Eliminating fictitious material is done by adding a penalty to the stiffness of intermediate density members. It was (Bendsøe and Sigmund 1999) who first created the SIMP (Solid Isotropic Material with Penalization) method to penalize the intermediate densities of elements, so that the solution was as close to binary as possible, as shown in **Equation 2**. $K_0{}^e$ represents the stiffness of a pure, solid element for element e and a SIMP factor of $\eta = 3$ was applied to the optimization in this work.

$$\mathbf{K}^e = \left((\rho^e)^\eta + \rho^e_{min}\right)\mathbf{K_0}^e$$

Equation 2 SIMP Penalty Function (Bendsøe and Sigmund 1999)

For this study, the optimization solution was not mesh-dependent, as a filter was applied to the elements. The default hex mesh could not be applied to the part because of its complex geometry. As a result, a free 'tet' mesh was applied to the part with an approximate global size of 0.06. This created 720,252 elements for the optimization, as shown in **Figure 22**.
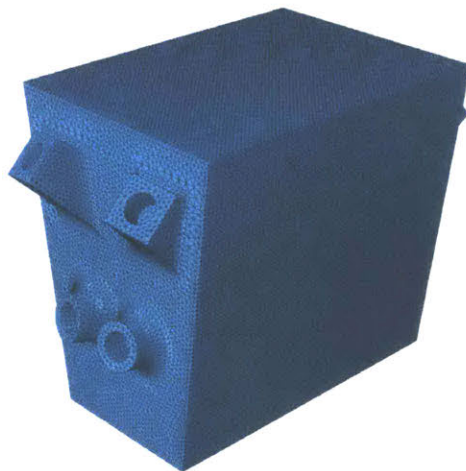
Figure 22 Design 'Tet' Mesh

Finally, after the optimizations were completed, the meshes were ready to be extracted as .stl files and imported back into Rhino to be prepared for fabrication. The surface meshes were extracted with the default settings of a 15° reduction angle with 5 smoothing cycles. Iso values were used to filter elements left over by the SIMP method. The default iso value was 0.3, so any remaining density elements up to 0.3 were discarded and the remaining elements with values above 0.3 were carried forward for the design. The iso values used for each specimen are shown in **Table 2**.

| Optimization - % Volume	20%	10%	7.5%
Iso Value	0.65	0.3	0.2

Table 2 Iso Values

The iso values of the extracted meshes were adjusted to help align the optimized connections' volume with a clean scale figure of the original connection. The trapezoidal design space had a much larger volume than the original connection, so the percent volume of the optimized parts varied depending on which it was compared to. The remainder of this study refers to the specimens as a percent volume with respect to the original connection as shown in **Table 3**.

With respect to Design Space	20%	10%	7.5%
With respect to Original Connection	100%	60%	50%

Table 3 Percent Volumes Translation

2.3 Fabrication

2.3.1 Mold Preparation
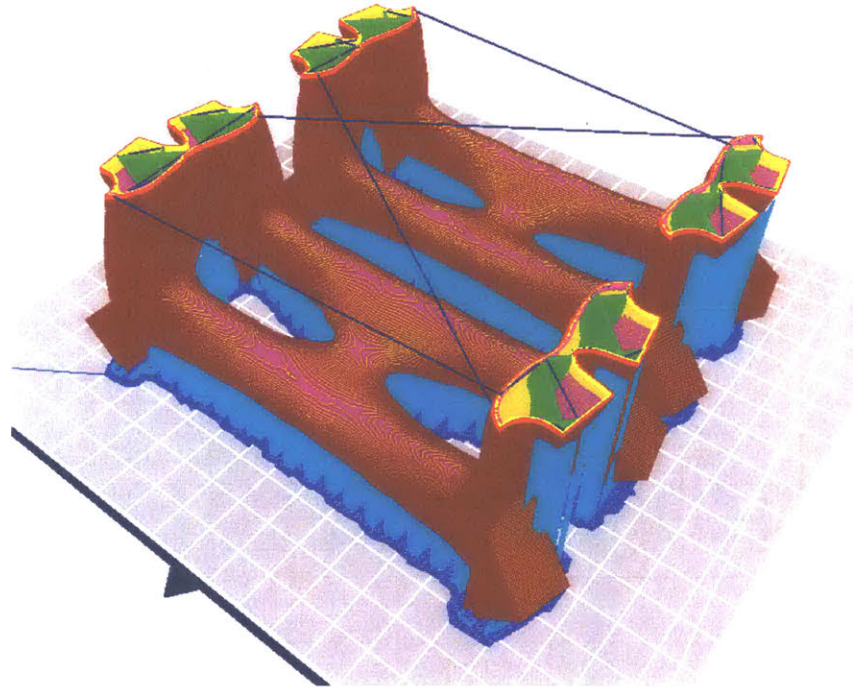
Figure 23 3D Print Setup of Initial Parts

       The conventional investment casting process and why it was chosen is discussed in **Section 1.2.3** This study modified the process by incorporating 3D printing into the beginning stages of casting in order to form the complex geometries of the connection. Initially, the parts were 3D printed out of white PLA with a thin shell of 0.8mm (shown in red), along with a mostly hollow structure of 5% infill (shown in green), and a layer height of 0.2mm. The minimal amount of material allowed for a quicker printing time, while reducing the amount of ash left behind when the part was burnt out. To minimize the support structure for the print (shown in cyan), which could deform the complex geometry, the parts were oriented upside down and printed in pairs as shown in **Figure 23**.

Figure 24 Investment Casting Wax Preparation

Red wax was then added to the part to act as the sprues and vents for metal to be poured into, as shown in **Figure 24**. The vents were essential to help minimize the shrinkage of the part while the liquid metal was cooling into its solid state. After the positive part was completely set, 910 glass-cast investment was mixed and poured around the part in order to form the negative mold, as shown in **Figure 25**. The mold was then placed in a furnace and heated to around 300° C to melt out the wax and PLA.

Figure 25 Glass-Cast Investment Mixed and Poured before Placing in Furnace

Wax would have been a more effective material to use as a positive, since it melts out cleanly and leaves a smoother finish. However, PLA was used for this experiment due to the scale and complexity of the parts needed. An issue with the PLA was that ash remained within the mold and needed to be blown out using the vents. After cleaning out the mold, the

furnace was raised to an extremely hot temperature of over 1200° C in order to turn the mold into a solid, ceramic state.

Another issue that had to be addressed throughout the molds was cracking. Due to the different material properties of the wax, PLA, and investment, each would expand differently under the intense heat, causing the mold to crack, as shown in **Figure 26**. To help mitigate this, chicken wire was integrated into the investment casting, acting similarly to rebar in concrete. After the mold had been cooled, metal sheets were wrapped and tied around the mold to help tighten it and prevent the liquid metal from leaking out.

Figure 26 Mold Cracking Mitigation

2.3.2 Investment Casting

An aluminum alloy of A356 was used for the casting, as it was easier and safer to handle than steel with the tools available in the MIT foundry. While the real connection is made out of welded steel, A356 is a strong, similar enough material to compare the strengths of the redesigned parts. In **Figure 27**, a mold is shown adjacent to the hydraulic crucible being prepared for the pour. The electromagnetic crucible used induction heating to raise the aluminum to around 700° C. This temperature was well above the melting point of A356 in order to ensure that the metal remained in a liquid state throughout the pouring of the entire mold, allowing it to cool evenly.

**Figure 27** Casting Post - Processing: Part Extraction

Once the metal had been poured, the mold took 4 to 8 hours to cool. After it had been cooled, the post-processing of the cast part begun with chiseling the aluminum part out of the ceramic mold, as shown in **Figure 27**. The sprues and vents were sawed off and sanded, leaving only the final, designed connection. After sandblasting the part, areas of improvement were highlighted throughout the part, mostly on the undersides. As shown in **Figure 28**, looking from underneath revealed porosity in the connection; this meant that there was not a clean pour of liquid metal. As described in further detail in **Section 3.2**, this problem pertained most visibly to the original parts. The topology-optimized redesigns appeared to have had small amounts of ash left in the molds prior to pouring.
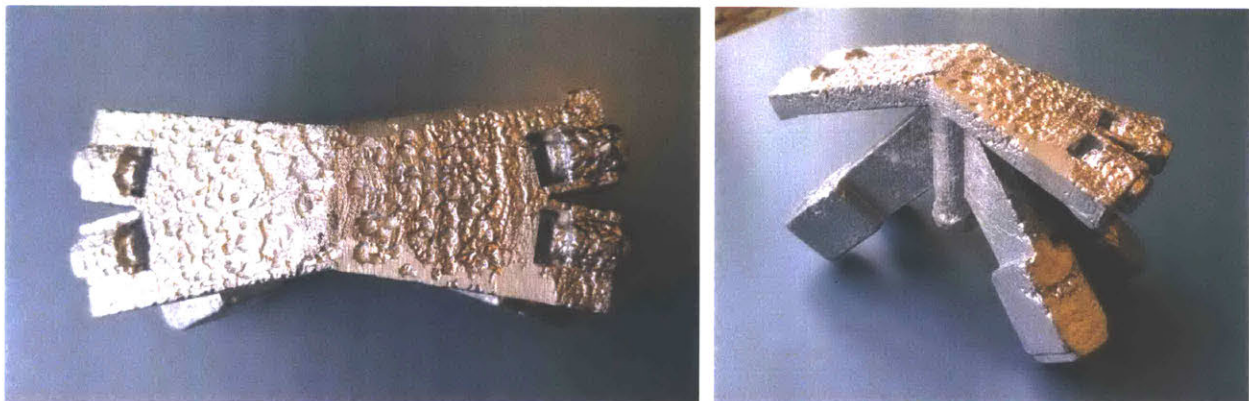
**Figure 28** Casting Porosity

2.4 Loading and Testing Frame Assembly
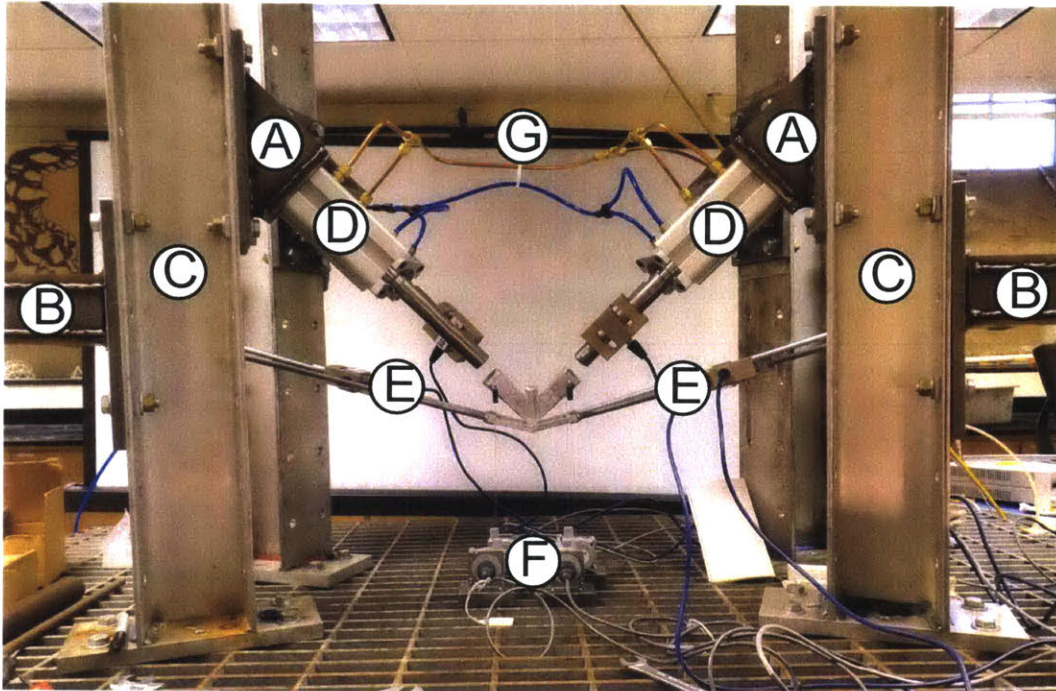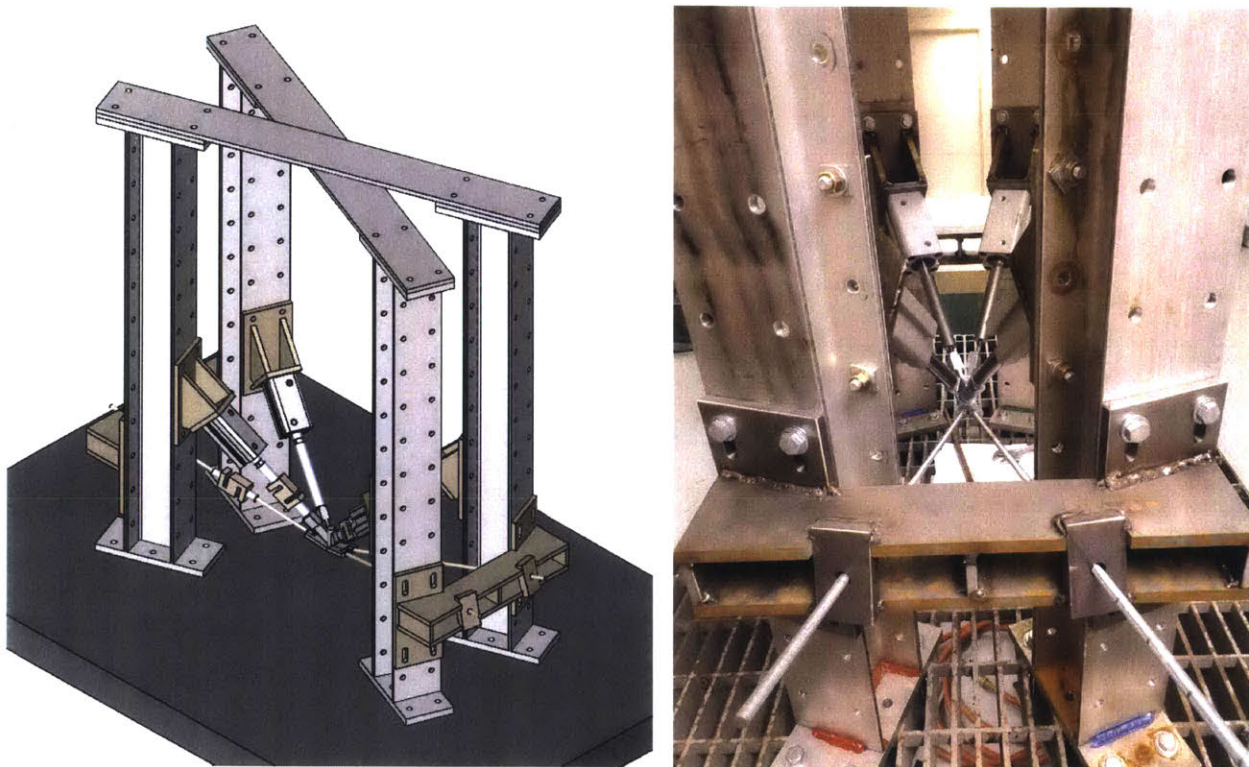

Figure 29 Testing Frame Assembly

The complex load case of the connection required a custom testing frame to be built. The testing frame was constructed as a multi-part assembly as shown in **Figure 29**. Most of the parts were milled and welded out of steel to ensure that the frame was stronger than the aluminum specimens. Part A is responsible for orienting the compression angles of the test, and Part B helps to orient the tension angles. Both parts are made out of ½" steel plates; the rectangular pieces are machined by hand and the angled pieces are made with a waterjet cutter to ensure precision, as shown in **Figure 30**. The vector created by these parts handles the angles in elevation necessary for the specimens.
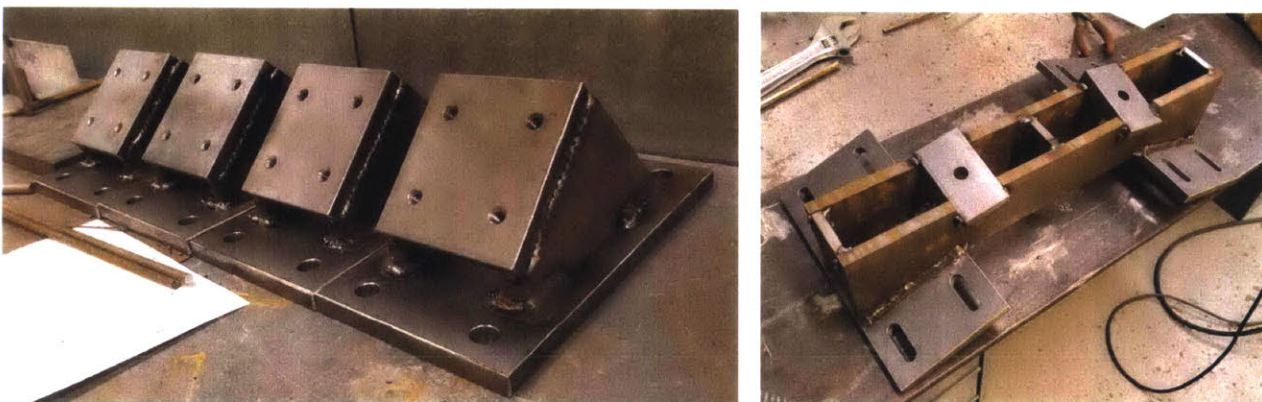
**Figure 30** Compression & Tension Plates (Parts A&B)

In order to then orient Parts A&B with the proper angle in plan, they are bolted to Part C, an aluminum wide flange beam, which is rotated on a steel table. To prevent Part C from bending as a cantilever from the table, aluminum plates are bolted on top across two aluminum wide flanges, as shown in **Figure 31**, so that the whole assembly is linked as a frame. As shown in **Figure 30**, the tension plates in Part B are more complex than the compression plates in Part A. This is because Part C is oriented to best accustom the angles of Part A. Since the compression and tension parts lay in different planes, as shown in **Figure 14**, Part B was fabricated as an adapter for the changing angles. Part B additionally has slotted holes milled into it to allow for vertical adjustability in the specimens to line up with the testing frame. The tensile plates are mounted behind the frame in order to use the strength of the aluminum beams in Part C, as shown in **Figure 31**. If Part B were to be mounted inside the frame, there would be less workability, and tension forces would be pulling away from the beams rather than into them.

Figure 31 Testing Frame Angles

To create loads on the specimens, hydraulic pistons are used in Part D, which are directly mounted and oriented by Part A, as shown in **Figure 29**. These pistons are powered by Part G, using oil supplied by the copper tubing to actuate the piston, and compressed air

37

supplied by the blue tubing to return the piston head to its original position. A PVA hydraulic pump is used, capable of producing 2000 psi of pressure. When combined with the 1.5" diameter piston's cylinder head from Part D, it is able to produce around 3.5 kips of load per piston. Since all four pistons in Part D are joined and hooked up to the same pump, an even load is assured across all the piston's cylinders. Two load cells are then added as an extension of the piston in order to measure and make sure the compression forces in the two planes are symmetric, as shown in **Figure 32**. Finished steel rods are then used to compensate for the remaining distance between the load cell and the specimen and to provide a smooth, finished face of contact.
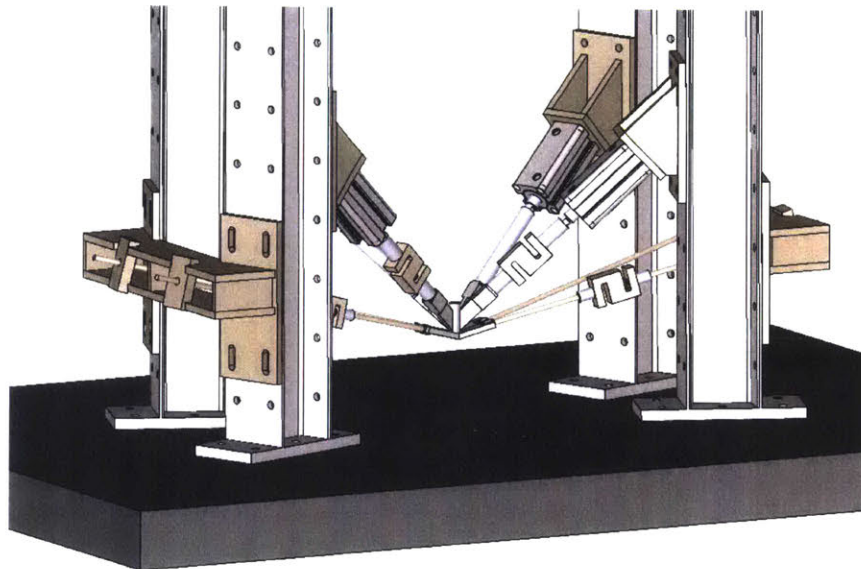
Figure 32 Load Cell Configuration

Part E consists of 3/8" threaded steel rods that would screw directly into the specimen and pass through the guided holes of Part B, as shown in **Figure 32**. Two more load cells are used in different planes to measure and make sure the tensile forces are symmetric. Before testing, each specimen is pre-loaded with 50-100lbs of tension to ensure that the entire system is tight before loading. Four string potentiometers are used in Part F, as shown in **Figure 29**, with a thin steel cable attached near the compression faces of the specimen to measure vertical displacements and calculate compliance.
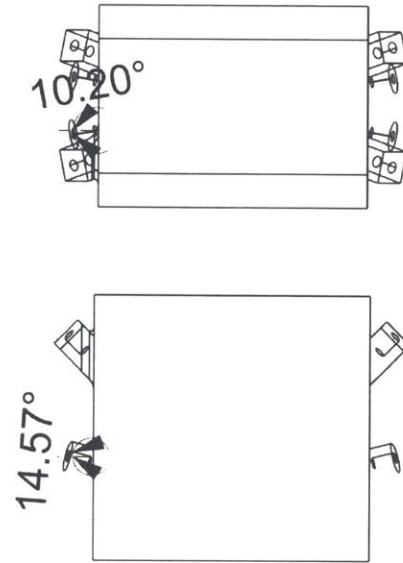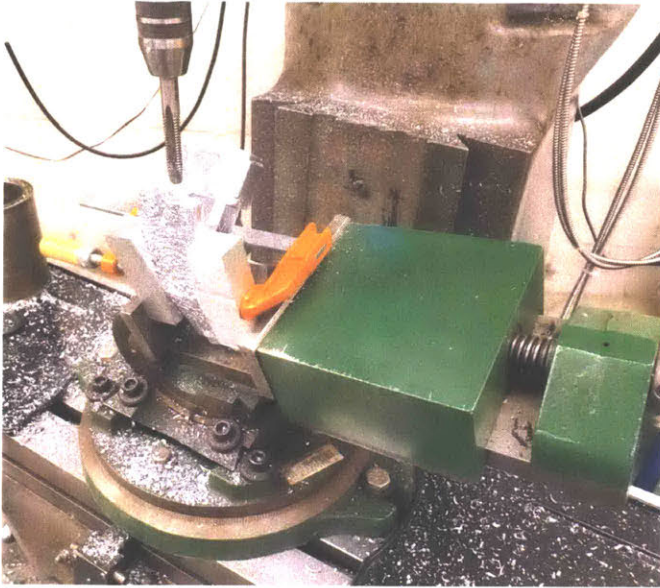
Figure 33 Tapping Threaded Holes into Specimens with a 3-Axis Tilting Vise

In this study, every specimen had to have threaded holes tapped into the tension faces to attach it into the testing frame. Because of the irregular geometry, a 3-axis tilting vise was used to orient the specimens in the milling machine and to make sure that all the angles were the same. As shown in **Figure 33**, there was an angle of 10.2° in plan and an angle of 14.6° in elevation for each specimen. A 3/8" diameter hole was tapped for Part E to screw into at a depth of ½" so that the rod would not strip the threads under load.

Figure 34 Original Eight Holes for Attaching Connection into Testing Frame

The original design intent was to tap threaded holes into the compression faces in addition to the tension faces. However, as shown in **Figure 34**, every specimen required eight holes that needed to line up perfectly to fit properly into the testing frame. Since the holes were being milled by hand, even with the 3-axis tilting vise, the manufacturing tolerances made it impossible for the specimen to fit properly; a few samples were used to verify this. To compensate for this issue, the remaining specimens eliminated the need for the compression rods from Part A to be screwed in. Instead, a butt joint was chosen so that the specimen would come directly into contact with the rods, as shown in **Figure 35**. Because the forces were still in compression, this altered contact between the specimen and the piston allowed the testing frame to be deemed sufficient for this study.


Figure 35 Fitting the Specimen into the Testing Frame

Results

The following discussion of results are broken up into three sections, continuing the process as discussed in **Section 2**. The first section discusses the optimized design results as produced by Abaqus with Tosca, and predicted modes of failure. The second section discusses the outcome of the investment casting as well as any material imperfections and variances. Finally, the third section discusses the load testing and how the data aligned with the computer simulation.

3.1 Design Results and Numerical Analysis

Original   100% Volume

60% Volume   50% Volume
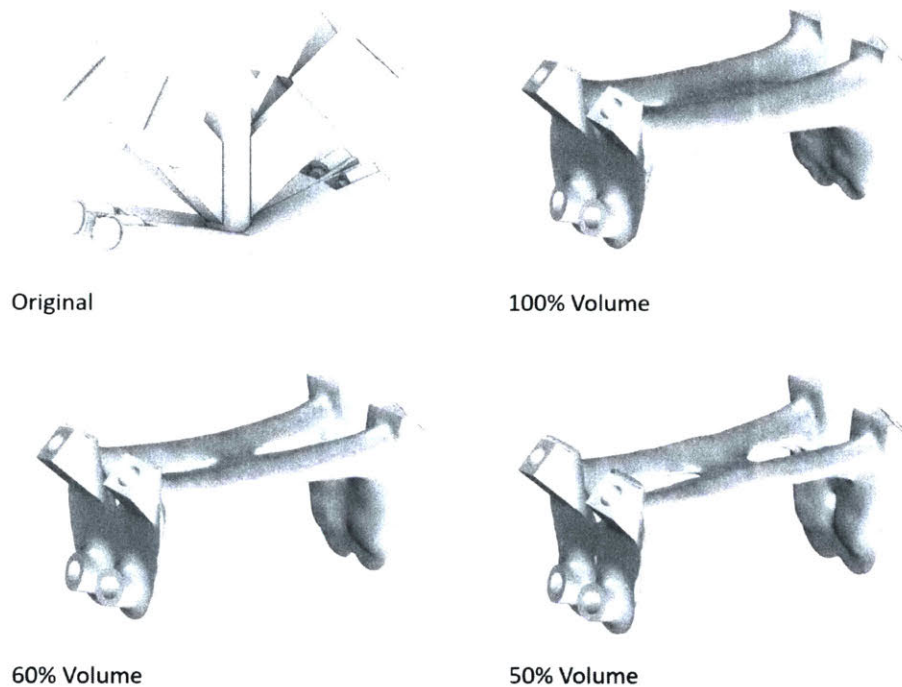
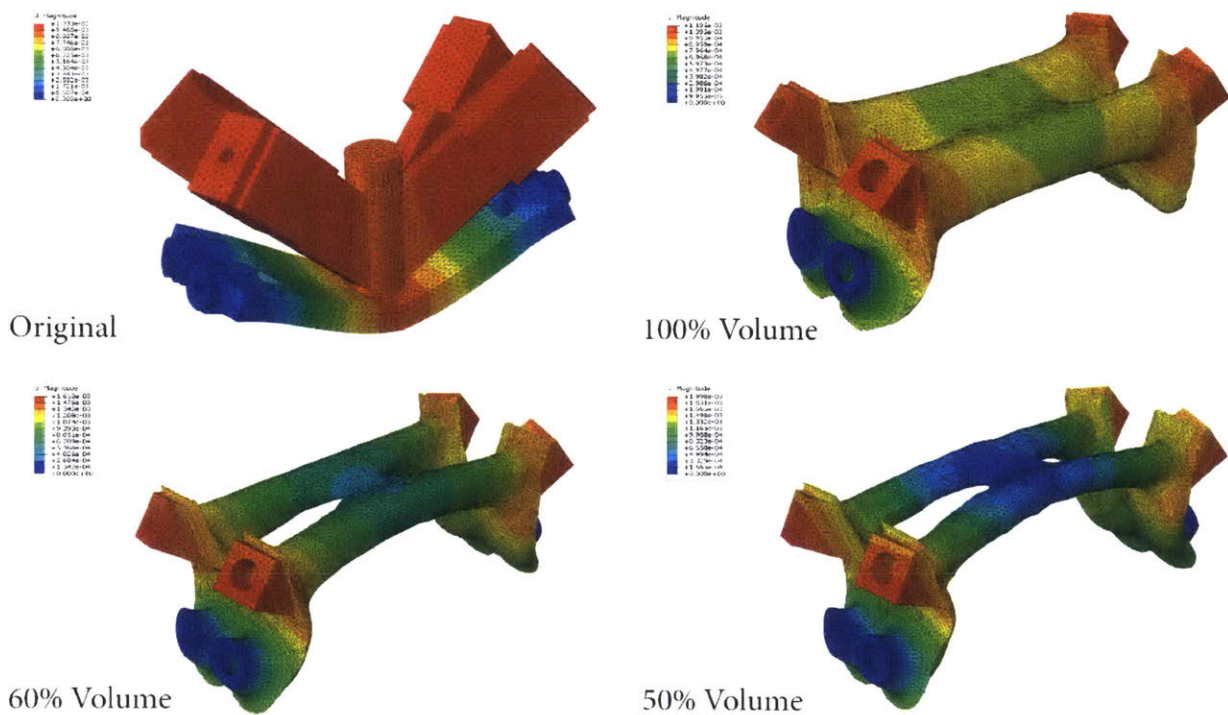**Figure 36** Topology Optimized Connections from Abaqus with Tosca

The optimized geometries, as a result from Abaqus with Tosca, are represented in **Figure 36**. The geometry was different than what was anticipated, as all the material was removed from the bottom portion of the connection. However, this makes sense as the support conditions for the tensile rods were modelled as pins, meaning that the connection would not displace but only rotate about the end plate, connecting the compression and tension forces. This allowed the geometry to become more free-form than the original connection while still falling within the manufacturing constraints of a minimum thickness

of 0.125". The general curvature and concavities were maintained throughout all the different optimized-designs, while internal voids were added into the connection for the 50% and 60% volume constraints. The 50% volume constraint was the lowest this study could perform before the optimization created a design that would have been unfeasible to manufacture.
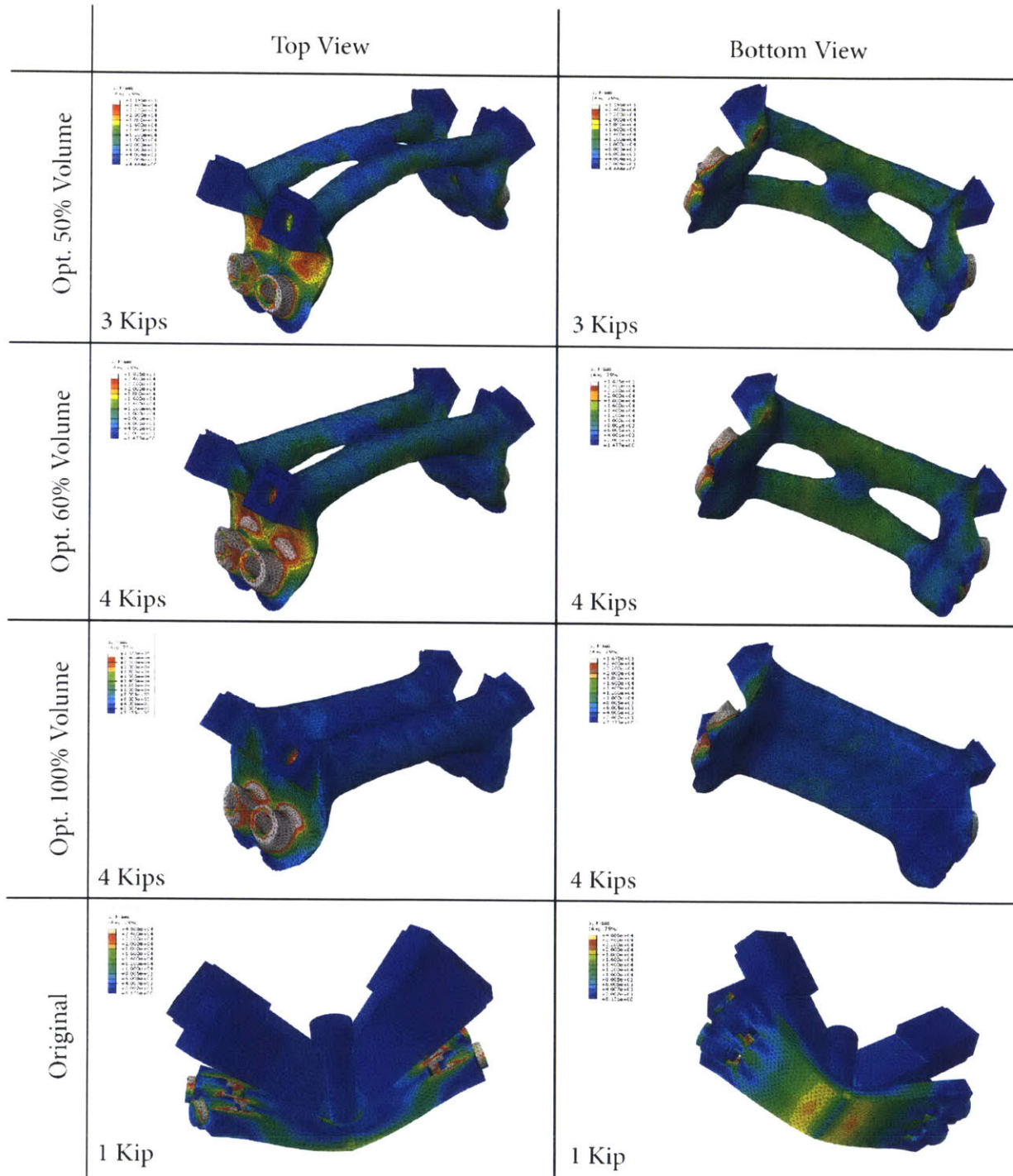
Figure 37 High Stress Areas and Predicted Failures of Optimized Connections (Abaqus)

As shown in **Figure 37**, an elastic Abaqus analysis shows the stress distribution amongst the different connections. The gray areas indicate high stress areas above 24,000psi, the yielding stress provided by ("Aluminum A356.0-T6, Sand Cast" 2019). These results work well for predicting where the connections would fail in the testing rig. Looking closely at the original connection, there appears to be local failure happening near where the tension rods screw into the part. The analysis shows the optimized connections perform as expected where the lower volumes are experiencing higher stresses than the higher volumes. Stress concentration builds up at the center of the end plate connecting the compression and tension forces. The centers of the optimized connections are experiencing mostly compression forces and do not appear to be yielding before the plate. The analysis also provides an indication about when the connections should begin to fail, around 1K for the original connection and around 3K-4K for the topology-optimized connections.

Original

100% Volume

60% Volume

50% Volume

Figure 38 Deflection of Optimized Connections at 1K Load (Abaqus)

To verify that the analysis model was accurate, deflections were checked, as shown in **Figure 38**. Within each component, the color scheme ranges from blue (lowest deflection) to red (highest deflection). The original connection shows clearest that the loads and supports are modeled correctly. The deflections are highest where the loads are applied, translating average deflections at the center of the connection, and ending with no

43

deflections at the pinned supports. The optimized connections tell a similar story, except the centers of the connections vary based on their volumes.

Deflection at 1K (Abaqus)
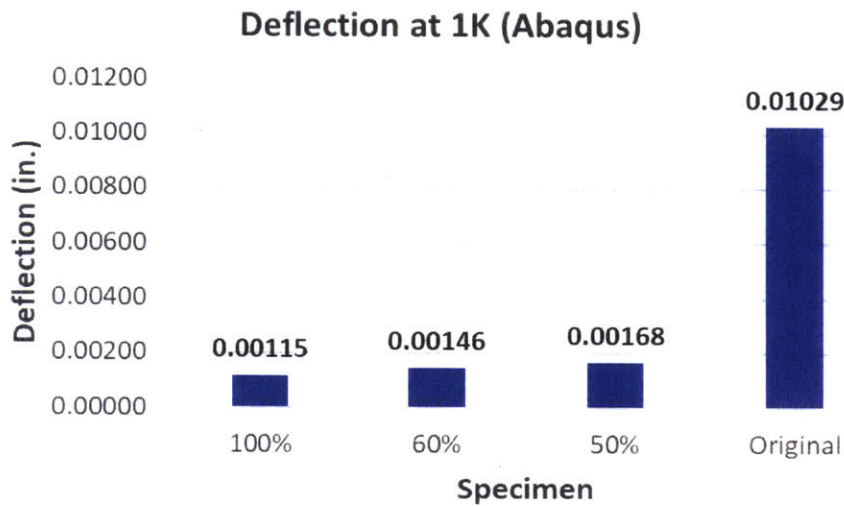
Figure 39 Deflection of Optimized Connections at 1K Load (Abaqus)

As a performance measure for the improvement of the topology-optimized connections over the original connection, **Figure 37** and **Figure 39** may be referred to. The optimized connections began to yield at around 3-4 times the load of the original connection. Not surprisingly, since designed for a compliance objective, the optimized connections appear to be stiffer as they deflect around 6-9 less than the original connection, as shown in **Figure 39**. Combining the better performance in both loads and deflections, the connections were expected to have a significantly higher performance than the original connection as discussed in **Section 3.3**.

3.2 Fabricated Design Results
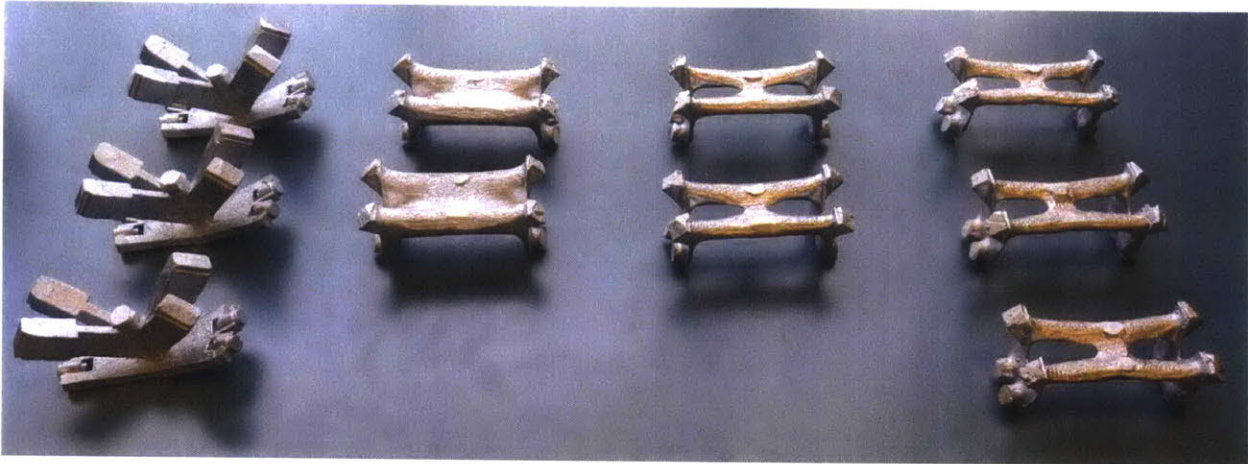
Figure 40 Cast Connections for Experimental Study

To account for unforeseen circumstances in manufacturing, three specimens were produced for each of the four types of connections. As a result from the casting, two molds failed and had the aluminum leak through the casing. The remaining 10 specimens were cleaned up, as shown in **Figure 40**, and were used in the remainder of this study for load testing. Across all the specimens, there was an imperfection in the center of the connections, where a small amount of metal was unable to be sanded off due to the free-form geometry. This extra metal was a result of the wax sprues used to help cast the connections as discussed in **Section 2.3.1.** As this was extra material for each specimen, it would not negatively affect their performances for load testing.
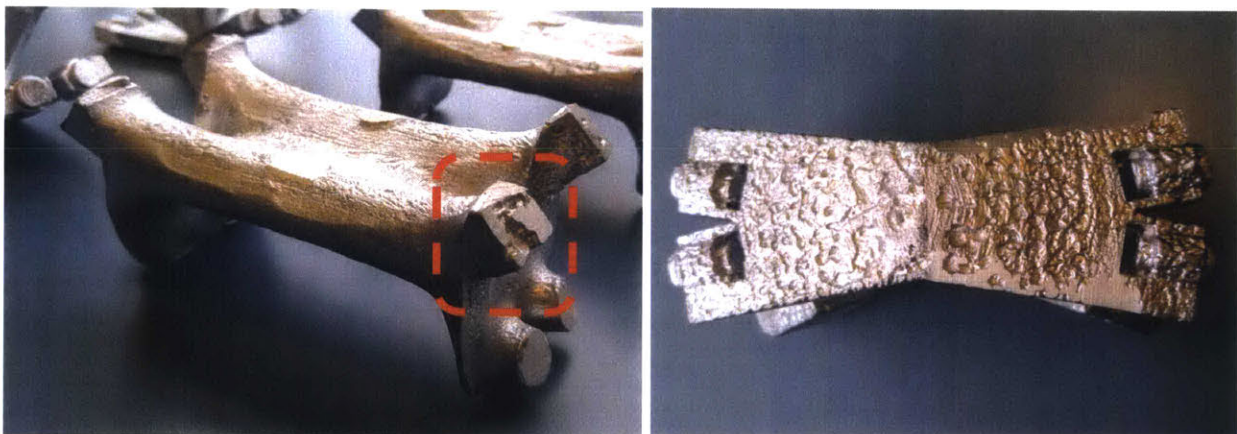
Figure 41 Casting Imperfections

There existed a porosity amongst the cast connections, most visibly seen in the original connection, as shown in **Figure 41**. The castings appeared to have had small

amounts of ash left in the molds prior to pouring. The ash was a result of the initial 3D printed PLA parts that were burned out to create the mold. To prevent this issue in a future study, the initial parts could be produced using a Stereolithography 3D printer to create wax parts that would burn out cleanly. The porosity existed more so in the original connection than the optimized redesigns due to the orientation they were casted in. As shown in **Figure 24**, the original connection was oriented horizontally with metal being poured in from the top, and the optimized redesigns were oriented vertically so that metal was poured in sideways. As a result, the complete bottom face of the original connection had porosity, while only the compression faces on one end of the optimized redesigns had porosity. However, this did not seem to affect the testing performance, as the connections did not fail in areas of visible porosity.

	Specimen	Comp. Holes?	Mass (lbs)	Density (lb/in³)	Physical Volume (in³)	Model Volume (in³)	% Volume Difference		% Mass Difference
Original	A1	N	0.8911	0.0965	9.234	10.653	87%		100%
	A2	N	0.8946	0.0965	9.271	10.653	87%		100%
	A3	N	0.8922	0.0965	9.246	10.653	87%		100%
Optimized	B1	N	0.9032	0.0965	9.360	10.546	89%		101%
	B2	N	0.8942	0.0965	9.266	10.546	88%		100%
	C1	Y	0.5232	0.0965	5.421	6.058	89%		59%
	C2	N	0.5606	0.0965	5.810	6.384	91%		63%
	D1	Y	0.4436	0.0965	4.597	5.100	90%		50%
	D2	N	0.4539	0.0965	4.704	5.426	87%		51%

Table 4 Cast Connections Volume Variations

Casting the connections resulted in material shrinkage from the cooling of the liquid aluminum, as shown in **Table 4**. The table is broken up to differentiate the original connection from the optimized redesigns. 'Comp. Holes?' stands for 'Compression Holes?' and explains that if a specimen had all eight holes tapped into it to connect to the testing frame as shown in **Figure 34**, this was taken into consideration when calculating the volumes. The density amounts shown in **Table 4** were provided by ("Aluminum A356.0-T6, Sand Cast" 2019). 'Physical Volume' represents the volume of the cast connections and 'Model Volume' represents what it was supposed to be as modeled in Abaqus. There is a consistent shrinkage for all of the casted connections of about 10%. More importantly, when comparing the optimized connections to the original connection, the percentage of mass

difference is consistent to what was implemented in the optimization; these percentages were volumes of 100%, 60%, and 50% as discussed in **Table 3**.

Figure 42 Punctured Hole in Optimized Connection

While tapping holes into the connections to fit them into the testing frame, a few specimens accidentally had the hole tapped too far in, leaving a puncture inside the optimized region of the connection as shown in **Figure 42**. This was due to the ½" depth needed in order to ensure that the threads of the tensile rod would not strip out of the connection, ruining the experiment. While cleaning the connections after they were casted, some parts were over-sanded, thus eliminating the depth needed for the thread. To prevent this issue in a future study, the boundary conditions should be extruded farther to account for shop error. This did not affect the testing performance, as the connections did not fail where the hole punctured through.
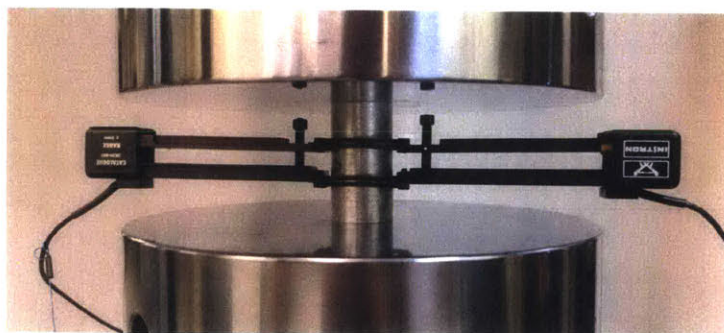
Figure 43 A356 Cylinder Load Testing

To verify that the material matched the material and mechanical properties of A356 as provided by ("Aluminum A356.0-T6, Sand Cast" 2019), cylinders of A356 made from the sprues of the cast connections were load tested, as shown in **Figure 43**. Four cylinders were tested, and their stress-strain results may individually be seen in **Figure 44**. Specimen A1 of

the cylinder tests demonstrated a homogenous material as the stress-strain curves line up perfectly. However, the other three specimens of the cylinder tests had varying strains at opposite sides of the cylinder, meaning that the material was heterogeneous. This was not an anomaly, as most of the tests had this feature and could be assumed that the connections may be heterogeneous. This may have been an adverse effect on the load testing due this casting imperfection. The imperfection may have been a result of the amount of air in the mold as the metal cooled, debris being mixed in with the liquid metal, or different cooling rates along the surface of the connection.
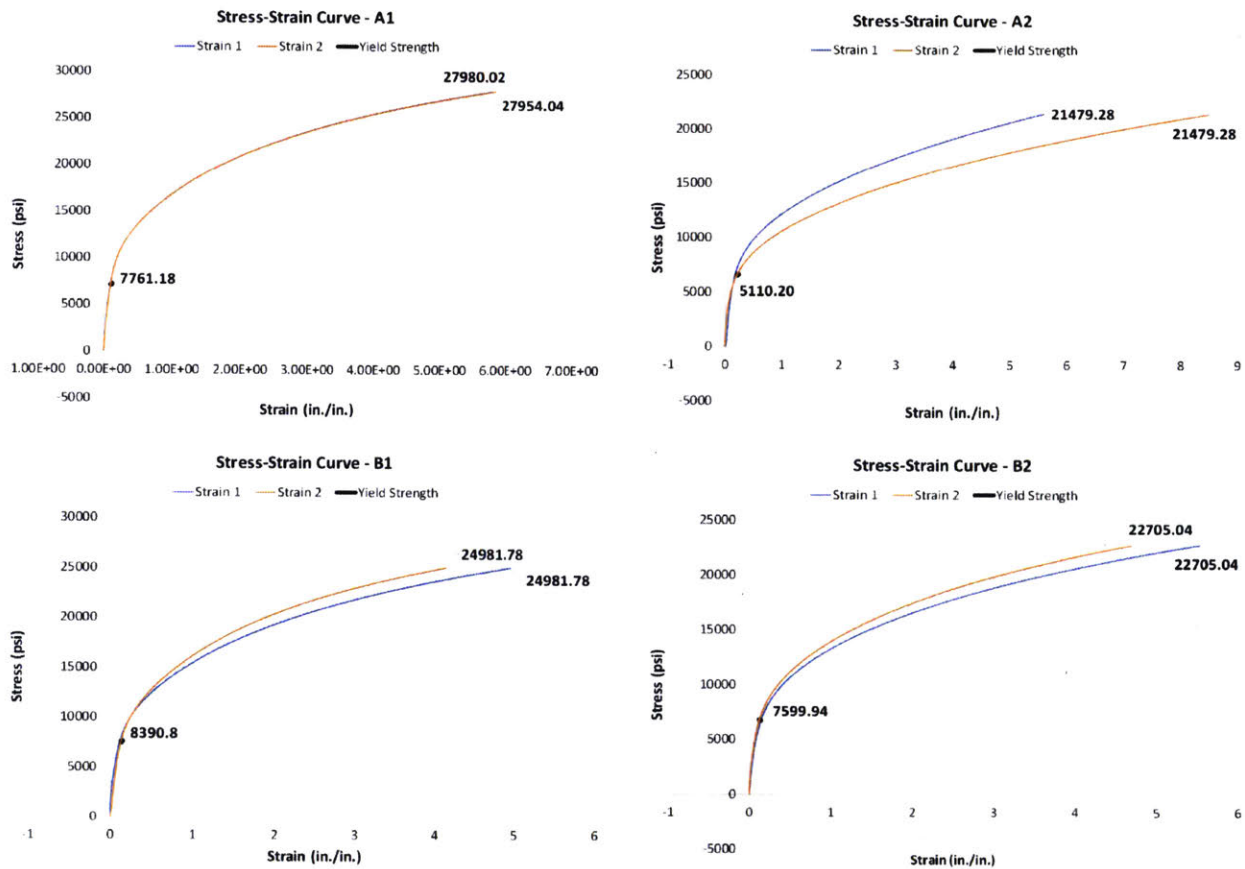
Figure 44 A356 Cylinders Stress-Strain Curves (Individual plots for each tested sample)

When overlaying all the obtained stress-strain curves together, the data from **Figure 45** shows how non-consistent the A356 material is. This may have negatively affected the load testing, as different specimens of the same type of connection would have inconsistent data. As shown in **Figure 46**, the Young's modulus and yield strength of the test cylinders were significantly different than those shown in **Figure 13**. There was an average yield strength of 7,200 psi for the testing cylinders, around a third of what was originally assumed.

48

The Young's modulus was around 70ksi for the testing cylinders, multiple orders of magnitude smaller than what was used in the design. These results demonstrate a significant flaw in the material properties used for the topology optimization. This may have been due to the specifications sheet provided by ("Aluminum A356.0-T6, Sand Cast" 2019) representing the metal after being heat tempered while the casted connections were not, resulting in significant strength differences. The A356 cylinder load testing revealed a significant factor that could negatively affect the load testing results. To prevent this issue in a future study, a more stable, consistent material is recommended to be tested beforehand with cylinder testing in order to verify the material's mechanical properties.
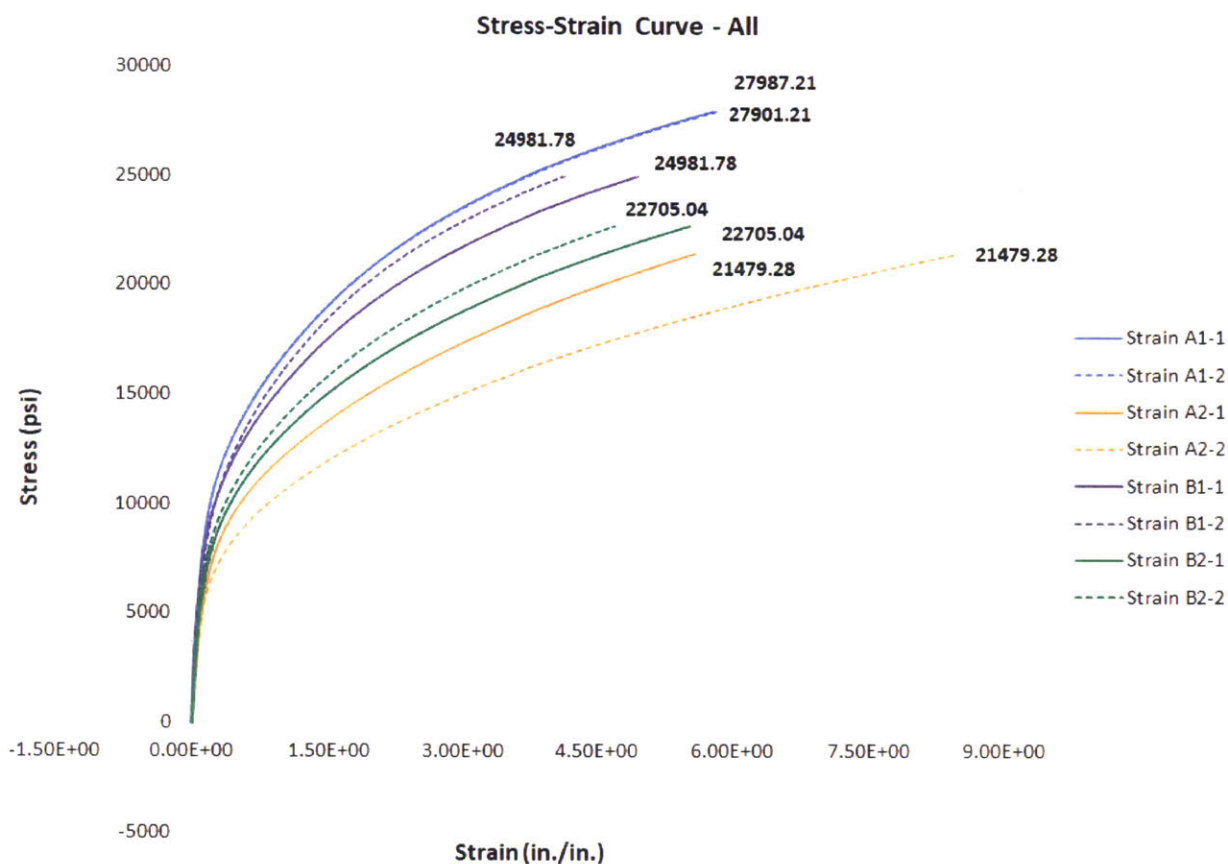
Figure 45 A356 Cylinders Stress-Strain Curves (Combined)

Young's Modulus

A1: 7.94E+01
A2: 5.25E+01
B1: 7.75E+01
B2: 6.95E+01

Young's Modulus (ksi) vs Specimen

Yield Strength

A1: 7761.2
A2: 5110.2
B1: 8390.8
B2: 7599.9

Yield Strength (psi) vs Specimen
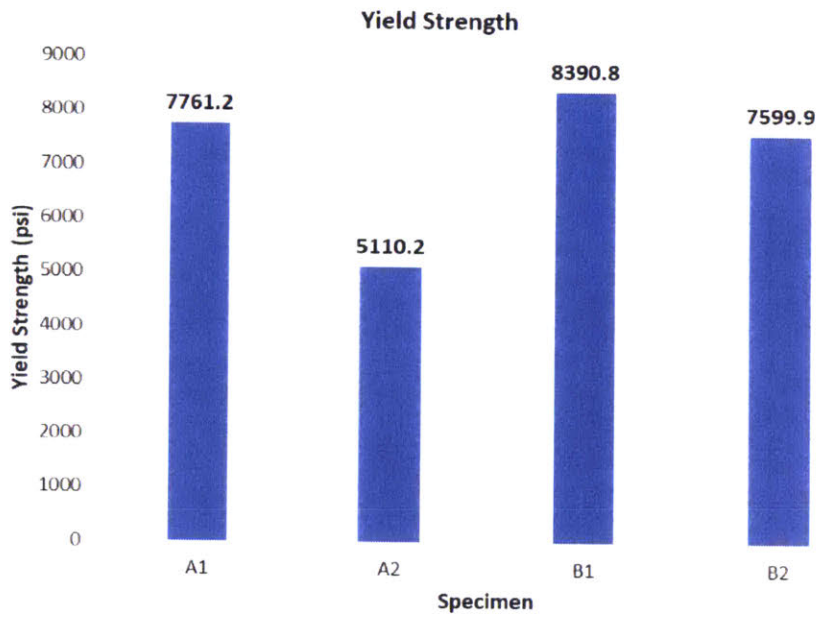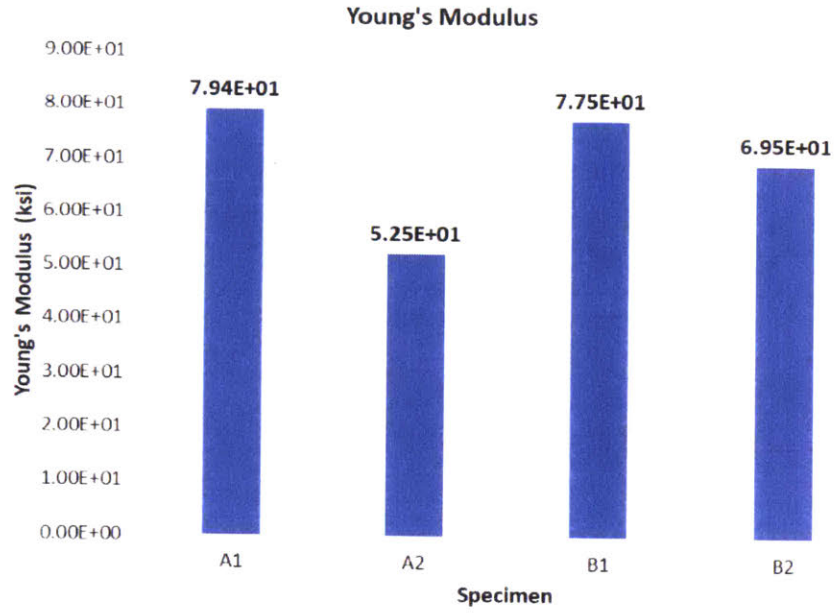
Figure 46 Young's Modulus and Yield Strength of A356 Cylinders

50

3.3 Load Testing & Verification
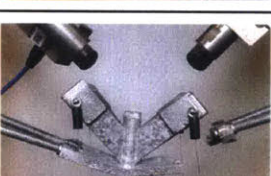
		Pre-Test	During Test	Post-Test
Opt. 50% Volume	D2			
	D1			
Opt. 60% Volume	C2			
	C1			
Opt. 100% Volume	B2			
	B1			
Original	A3			
	A2			

Figure 47 Catalog of Images for Specimens Before, During, and After Load Testing

A collection of images displaying the connections before, during, and after the load testing is shown in **Figure 47**. In the 'Pre-Test' column, the connections are shown individually, with all the tapped holes created after they were cast. The tapped holes include those in the tension faces of all the specimens and the compression faces of a few specimens. There is also a miniscule hole tapped into the side of the compression faces for the string potentiometers to screw into and measure displacements. This can be seen in the 'During Test' column and is further explained in **Section 2.4.** This did not affect the testing performance, as the connections did not fail where the tapped holes were made. For the rest of this study, the specimens are renamed for the load testing purposes herein and are shown in **Figure 47** and **Table 5**.

Connection Type	Original	Opt. 100%	Opt. 60%	Opt. 50%
Specimen Label	A	B	C	D
No. of Specimens	3	2	2	2

Table 5 Specimen Naming Schemes

The performance of the four types of specimens are presented in **Figure 48**. The slopes of the graphs are consistent among the different parts, implying that the stiffness was the same for each respective specimen type. The graph also shows a large amount of jitter throughout the tests for the optimized connections. This is due to slippage of the piston coming into contact with the specimen as more load is applied. There is little to no slippage in the original connection, as the specimen has a larger surface area that came into contact with the piston as well as a clean, smooth surface. The optimized connections have a small, square face that was uneven due to porosity and over-sanding in the manufacturing process, as discussed in **Section 3.2.** To prevent this issue in a future study, the compression face of the specimen should be larger than the head of the piston, and the part should be oriented in such a way during casting so that porosity would not become an issue.
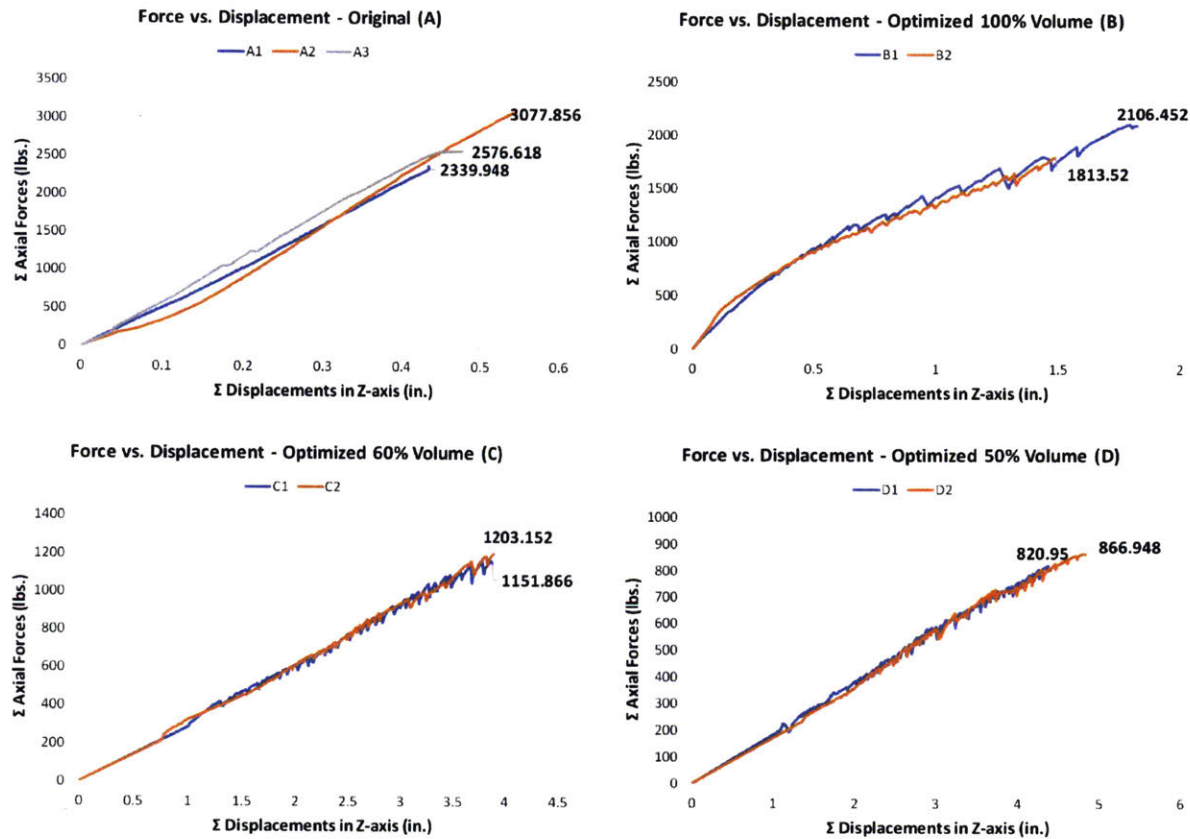
Figure 48 Sum of Forces vs. Sum of Displacements for Experimental Study (Individual plots for each type)

Most of the specimens experienced a brittle failure with minimal to no ductility, as shown in **Figure 49**. The graph shows that the displacements are much higher than what was predicted by the Abaqus model. The large variance in displacements is most likely due to the lower-than expected volume of each casted part and the lower Young's modulus of the material as discussed in **Section 3.2**. However, the pinned support conditions that were used to model the optimization may also have contributed. Within the experiments, it was observed that the connections were rotating slightly about the tension face downwards, displacing at the pins. The downwards displacement can be seen more clearly in Specimen D from **Figure 47**. Specimen D is shown displacing so much that the piston came into minimal contact with the connection, and nearly completely slipped off.

Even though the load can increase at a constant rate and constant direction, no matter how much surface area was in contact between the compression face and the piston, the position of the load changed over time. This could have had a significant impact on the load testing, as the specimen began acting like a beam with opposing moments being applied on

53

each end. As a result, the optimized redesigns failed mostly near the center of the connection, with the exception of Specimen B1, rather than on the end plate connecting the compression and tension forces as predicted. This can be clearly seen in the 'Post-Test' column of **Figure 47**, with the failures occurring where the cross-sectional area of the connection was the smallest. The figure also shows that the original connection failed similarly to where the Abaqus model predicted; a local failure occurred near where the tension rods screw into the part. To prevent the issue of a moving load in a future study, a bracket could be made so the that the piston may come into face-to-face contact with the connection, eliminating its ability to slip and displace, as was observed for Specimens B-D.
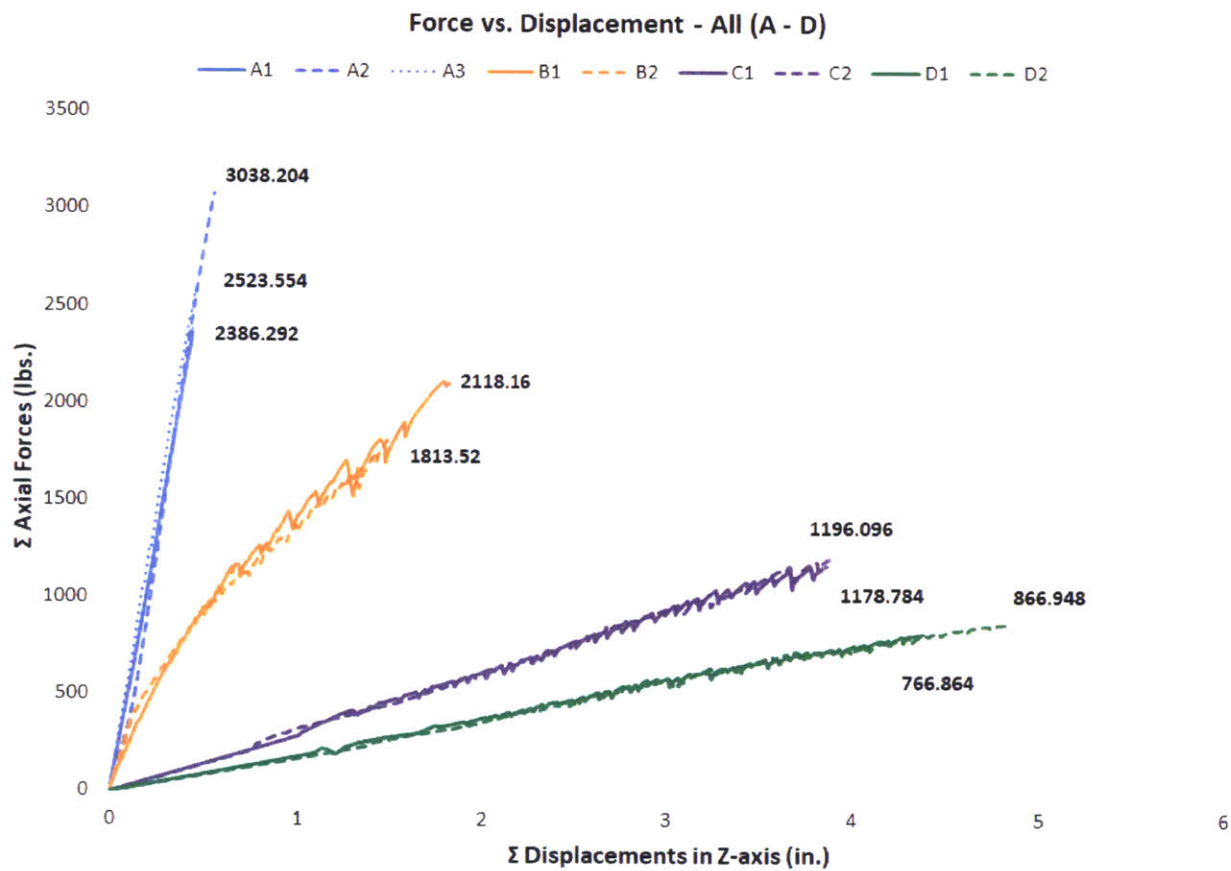
Figure 49 Sum of Forces vs. Sum of Displacements for Experimental Study (Combined)

When comparing the overall performance results, as shown in **Figure 49**, the graph shows that the optimized connections significantly underperformed as to what was expected. The original connection outperforms all of the optimized redesigns, as shown in **Figure 50**. The ultimate load of the original connection was about 50% of what was

predicted through the Abaqus analysis. The optimized connections performed only around 12.5% of what was expected with Abaqus. This large variance between the experimentation and Abaqus may be due to the volume shrinkage, support conditions, and inconsistent material properties as discussed in **Section 3.2.**

Despite these variances, the data is still comparable from one specimen to another, even though it is not directly comparable to the Abaqus results as described in **Section 3.1.** The graph in **Figure 50** shows a comparison of the average ultimate loads for each type of connection. Specimen C (Opt. 60%) has a possible proportional stiffness to Specimen B (Opt 100%), as the ultimate load of 1,184.4 lbs. in Specimen C is around 60% of the 1,960 lbs. in Specimen B, with 60% of the volume respectively. Stiffness is no longer proportional below Specimen C (Opt. 60%), as the ultimate load has a greater reduction when more volume is removed.

Ultimate Loads - Optimized Volumes
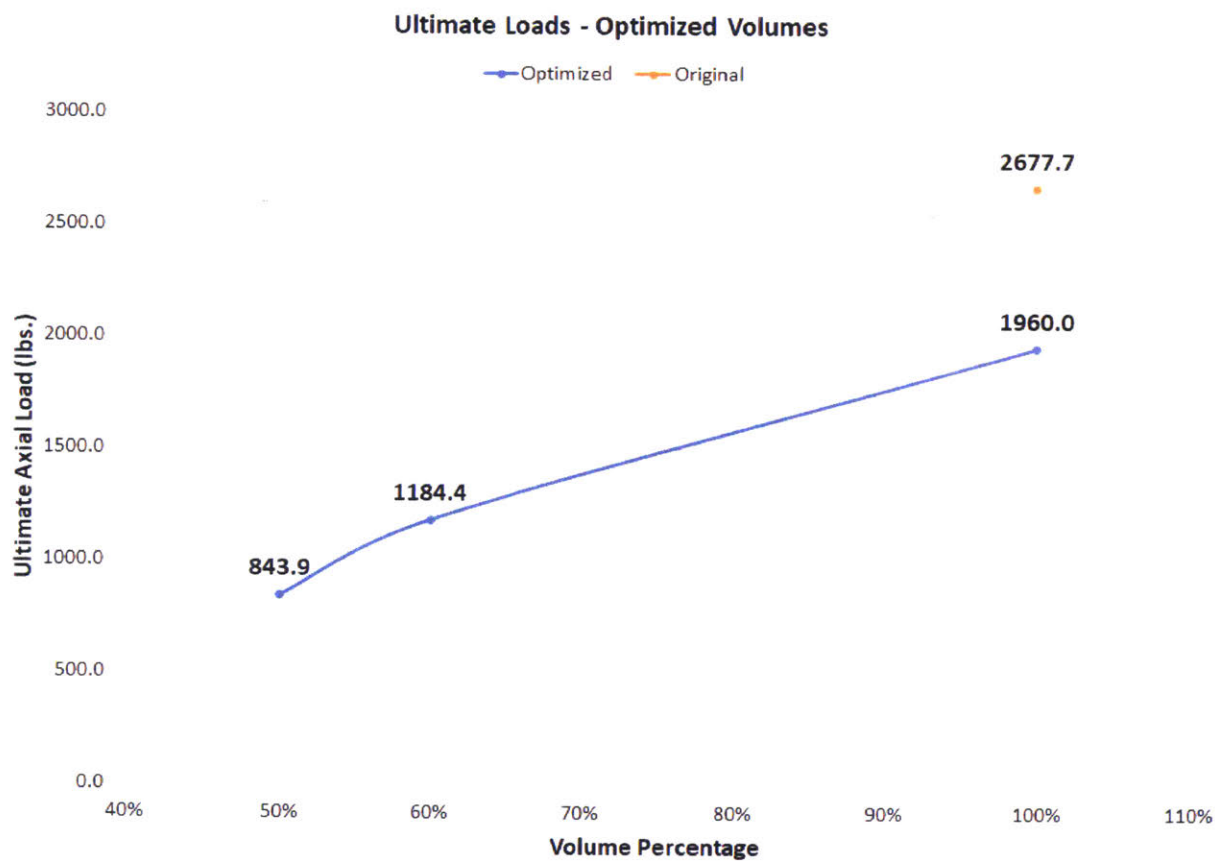
Figure 50 Ultimate Loads for Experimental Study

The final verification from the experiment arises from the design objective of the optimization to minimize the compliance within the connection. **Figure 51** shows that the compliance goes in opposite directions when comparing the Abaqus model to the experiment. The graph shows an upward trend moving from the original connection to the optimized redesigns for the experiment results. There is an opposite trend in the Abaqus results, as the compliance for the optimized results should have been significantly smaller than that of the original connection. The compliance of the original connection was around four times greater for the experiment than in the Abaqus model. The compliance of the optimized connections was multiple orders of magnitude greater for the experiment than in the Abaqus model. This shows how sensitive the optimization is to establishing the correct material properties, boundary conditions, and volume constraints as discussed in **Section 3.2.**

Compliance @ 200lbs
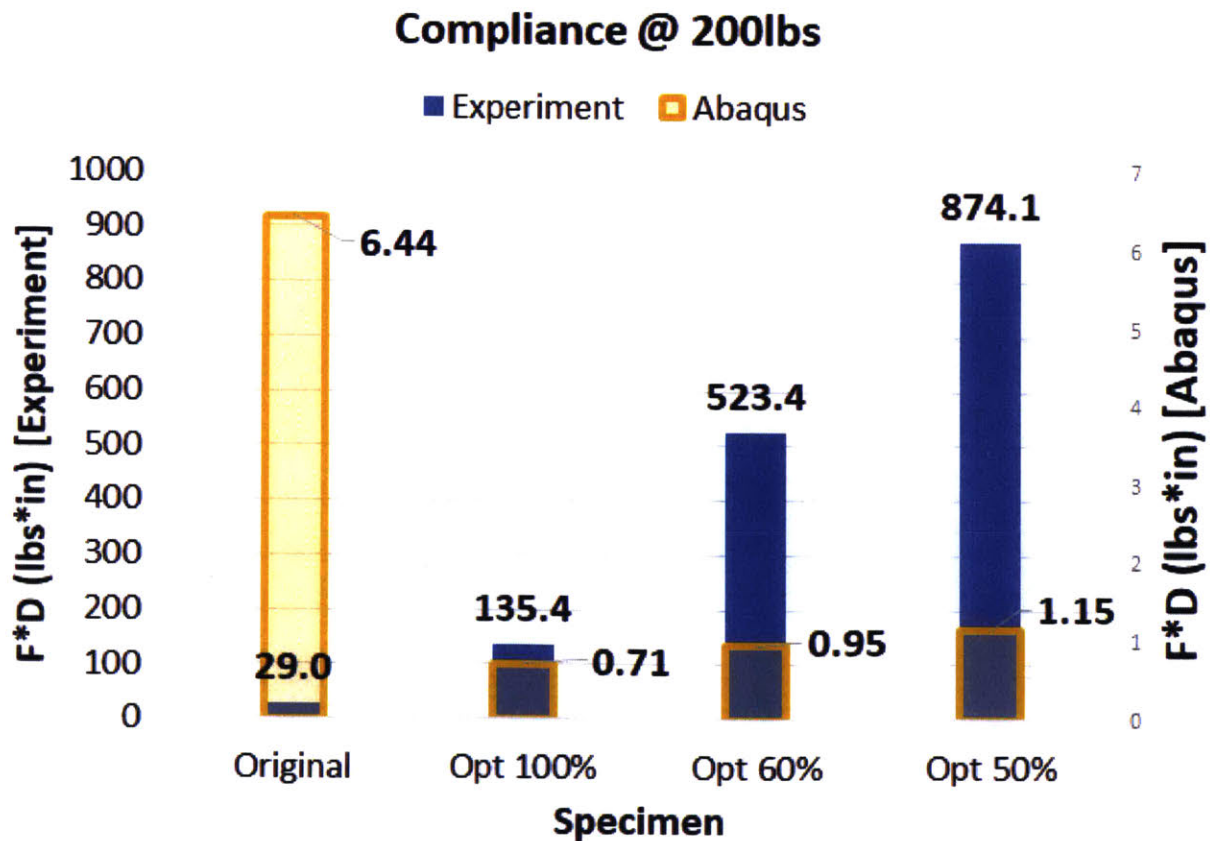
■ Experiment   ▫ Abaqus

Figure 51 Compliance at 200 lbs. for Experimental and Abaqus Study

Conclusion

4.1 Summary

This thesis proposes a study aiming to bridge the gap across disciplines by designing a topology-optimized building connection, finding an effective method to fabricate the design, and experimentally load-test its behavior to verify the performance results. A roof truss connection is chosen from the Scottish Parliament in Edinburgh as it is a unique node joining eight elements (four in compression and four in tension) in an unordinary truss. The connection is simple enough to be symmetrical both in the x-axis any y-axis, but complex in its angularity in both planes. Not only does the connection perform well structurally, but it is also highlighted architecturally throughout the debating chamber.

Abaqus is chosen as the commercial software used for the design in this work because it provides a built-in finite element analysis (FEA) software as well as Tosca with topology optimization. An elastic continuum topology optimization is set up using the Tosca engine with a density-based approach. The specified objective for the test is to minimize the global compliance, which then maximizes the stiffness of the connection subject to a varying volume constraint. Manufacturing constraints are also taken into consideration, as provided by an A356 specifications sheet and a feasible length scale for casting. The optimization and analysis indicate significant material savings in addition to performance improvements.

The connections then undergo the process of being investment cast out of aluminum in the MIT foundry. An aluminum alloy of A356 is chosen for the casting, as it is easier and safer to handle than steel with the tools available in the MIT foundry. While the Scottish Parliament Connection is made out of welded steel, A356 is a strong, similar enough material to compare the strengths of the redesigned parts. The conventional casting process is modified by incorporating 3D printing into the initial formwork to help create the free-form geometries resulting from the topology optimization. The complex load case of the connection requires a custom testing frame to be built. The testing frame is constructed as a multi-part assembly, where most of the parts are milled and welded out of steel to create the custom angles representing the roof truss.

There are many challenges associated with testing physical specimens in the field of structural engineering. The casted material in this work contains many imperfections, such as its yield stress and Young's modulus significantly underperforming compared to what is stated in the specifications sheet. This may be due to the absence of heat tempering after the connections were casted. There is also a consistent 10% material shrinkage in the casted connections that was not accounted for in the design.

While the experimental results are not directly comparable to the Abaqus results due to the conflicting stories they tell, the experimental specimens themselves are comparable. No computer simulation can directly replicate a load testing setup. As a result, there was a significant amount of slippage during the tests, allowing the applied loads to be moved along the connection. This changed the failure location to the center of the connections rather than the end plates as predicted in Abaqus. Most of the specimens experienced a brittle failure with minimal to no ductility.

The results of the experiment saw the original connection as the strongest specimen for the ultimate loads, stiffness, and compliance. The optimized connections performed only around 12.5% of what was expected for the ultimate load, while the original connection performed about 50% of what was expected. However, there may be a proportional stiffness between the optimized specimens, as the ultimate load was directly proportional to the amount of volume removed. The compliance of the optimized connections was multiple orders of magnitude greater for the experimentation than in the Abaqus model, while the original connection was only four times greater. Overall, the original connection more closely aligned to the Abaqus analysis than the optimized connections.

This study shows how sensitive the optimization is when establishing the correct material properties, boundary conditions, casting process, and volume constraints. This study also provides the first iteration of the design process for creating a topology-optimized connection that performs the same in physical experimentation as it does computationally. Lessons can be taken from this and applied to the next iteration of this design.

4.2   Future Work

There are several framework limitations that may be improved for a future study. First, improvements in the fabrication are discussed. If the connections are to be made out metal with investment casting, the initial parts could be produced using a Stereolithography 3D printer to create wax parts that would burn out cleanly from the mold. The part should also be oriented in a way during casting so that porosity would not become an issue. In addition, there exists the possibility of 3D printing the metal directly using direct metal laser sintering (DMLS) or laser powder bed fusion (LPBF) technologies. The specimens could also be made from subtractive manufacturing using a fix-axis CNC milling machine. However, a more consistently stable material may be desired for the experimentation, such as plastic. Cylinder testing should also be completed beforehand in order to verify the material's mechanical properties.

Secondly, improvements in the testing rig are discussed. The boundary conditions should be extruded farther to account for manufacturing error when fitting the connection into the testing rig. This will help prevent the tapped holes from puncturing through the optimized region. In addition, the compression face of the specimen should be larger than the head of the piston with a custom joint to secure the two faces. This will help to prevent slippage throughout the experimentation while also keeping the load in a constant position and direction, similar to actual roof truss loads.
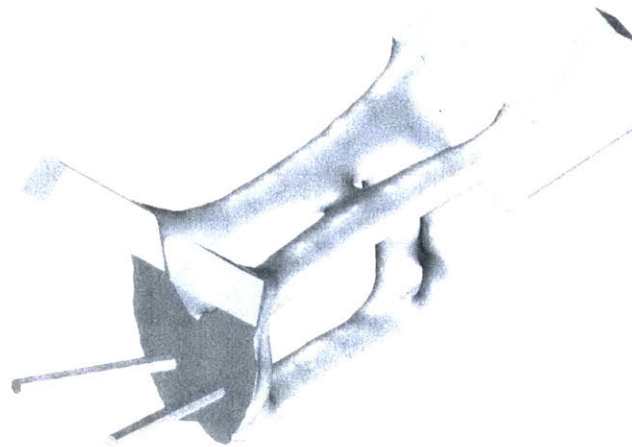
Figure 52 Re-Optimized Connection with Modified Boundary Conditions (Pin-Roller)

59

Finally, an improvement in the topology optimization process is discussed. A simple change can be implemented to the optimization that would result in a dramatically different re-design. The original boundary conditions were modeled as pinned supports, only allowing for rotation at the tension face. However, this was not the case in experiment, as discussed in **Section 3.3** when the specimens displaced significantly downwards. The supports should be less restraining for displacements in the z-direction for a future study. An example of what a re-optimized connection may look like with a pin-roller configuration is shown in **Figure 52**, where material is added to the bottom of the connection to better resist the tensile forces.

While there appears to be much room for improvement, this study provides the methodology for conducting topology optimization of an external building connection, while verifying the computational simulation through a physical experiment.

References

"Abaqus Analysis User's Guide." 2014. In *Abaqus 6.14 Online Documentation*. Dassault Systemes. https://www.sharcnet.ca/Software/Abaqus/6.14.2/v6.14/books/usb/default.htm.

"About The Building." 2014. The Scottish Parliament. June 19, 2014. https://www.parliament.scot/visitandlearn/9983.aspx.

Addaero. 2016. http://addaero-mfg.com/.

Alexandersen, Joe, Ole Sigmund, and Niels Aage. 2015. "Topology Optimisation of Passive Coolers for Light-Emitting Diode Lamps," 6.

"Aluminum A356.0-T6, Sand Cast." 2019. 2019. http://www.matweb.com/search/datasheet_print.aspx?matguid=d524d6bf305c4ce99414cabd1c7ed070.

Bendsøe, M. P., and O. Sigmund. 1999. "Material Interpolation Schemes in Topology Optimization." *Archive of Applied Mechanics (Ingenieur Archiv)* 69 (9–10): 635–54. https://doi.org/10.1007/s004190050248.

Bendsoe, Martin Philip, and Ole Sigmund. 2004. *Topology Optimization: Theory, Methods, and Applications*. 2nd ed. Berlin Heidelberg: Springer-Verlag. https://www.springer.com/us/book/9783540429920.

Boake, Terri Meyer. 2015. *Architecturally Exposed Structural Steel: Specifications, Connections, Details*. Basel: Birkhäuser.

Bruggi, Matteo. 2009. "Generating Strut-and-Tie Patterns for Reinforced Concrete Structures Using Topology Optimization." *Computers & Structures* 87 (23–24): 1483–95. https://doi.org/10.1016/j.compstruc.2009.06.003.

Bruns, Tyler E., and Daniel A. Tortorelli. 2001. "Topology Optimization of Non-Linear Elastic Structures and Compliant Mechanisms." *Computer Methods in Applied Mechanics and Engineering* 190 (26): 3443–59. https://doi.org/10.1016/S0045-7825(00)00278-4.

Carter, W.T., D.J. Erno, D.H. Abbott, C.E. Bruck, G.H. Wilson, J.B. Wolfe, D.M. Finkhousen, A. Tepper, and R.G. Stevens. 2014. "The GE Aircraft Engine Bracket Challenge: An Experiment in Crowdsourcing for Mechanical Design Concepts." In , 1402–11. http://sffsymposium.engr.utexas.edu/sites/default/files/2014-110-Carter.pdf.

Chaparro, B. M., S. Thuillier, L. F. Menezes, P. Y. Manach, and J. V. Fernandes. 2008. "Material Parameters Identification: Gradient-Based, Genetic and Hybrid Optimization Algorithms." *Computational Materials Science* 44 (2): 339–46. https://doi.org/10.1016/j.commatsci.2008.03.028.

Done, Brad. 2016. "What's the Difference Between Investment Casting and Sand Casting?" Machine Design. April 21, 2016. https://www.machinedesign.com/metals/what-s-difference-between-investment-casting-and-sand-casting.

Galilei, Galileo. 1638. *Dialogues Concerning Two New Sciences*. https://ebooks.adelaide.edu.au/g/galileo/dialogues/.

Galjaard, Salomé, Sander Hofman, Neil Perry, and Shibo Ren. 2015. "Optimizing Structural Building Elements in Metal by Using Additive Manufacturing," 12.

García-Domínguez, A., J. Claver, and M.A. Sebastián. 2017. "Study for the Selection of Design Software for 3D Printing Topological Optimization." *Procedia Manufacturing* 13: 903–9. https://doi.org/10.1016/j.promfg.2017.09.155.

Gatto, Andrea, Luca Iuliano, Elena Bassoli, and Maria Grazia Violante. 2007. "3D Printing Technique Applied to Rapid Casting." *Rapid Prototyping Journal* 13 (3): 148–55. https://doi.org/10.1108/13552540710750898.

Gibson, I., D. W. Rosen, and B. Stucker. 2015. *Additive Manufacturing Technologies: 3D Printing, Rapid Prototyping and Direct Digital Manufacturing.* Second edition. New York ; London: Springer.

Guest, J. K., J. H. Prévost, and T. Belytschko. 2004. "Achieving Minimum Length Scale in Topology Optimization Using Nodal Design Variables and Projection Functions." *International Journal for Numerical Methods in Engineering* 61 (2): 238–54. https://doi.org/10.1002/nme.1064.

Jewett, Jackson. 2018. "Design, Fabrication, and Testing of Plain Concrete Beams Using Topology Optimization." 2018. https://dspace.mit.edu/handle/1721.1/120634.

Menges, Achim, Bob Sheil, Ruairi Glynn, and Marilena Skavara. 2017. "RETHINKING DESIGN AND CONSTRUCTION," 7.

Michalek, Jeremy, Ruchi Choudhary, and Panos Papalambros. 2002. "Architectural Layout Design Optimization." *Engineering Optimization* 34 (5): 461–84. https://doi.org/10.1080/03052150214016.

Michell, Anthony. 1904. "The Limits of Economy of Material in Frame-Structures." *Philosophical Magazine*, 1904.

Molsheim, and Wolfsburg. 2018. "BUGATTI DEVELOPS WORLD'S LARGEST TITANIUM FUNCTIONAL COMPONENT: PRODUCED BY ADDITIVE MANUFACTURING." January 22, 2018. https://www.bugatti.com/media/news/2018/world-premiere-brake-caliper-from-3-d-printer/.

Mueller, Caitlin, and John Ochsendorf. 2013. "From Analysis to Design: A New Computational Strategy for Structural Creativity." In .

OptiStruct. 2019. Altair. https://altairhyperworks.com/product/optistruct.

Sigmund, O., and J. Petersson. 1998. "Numerical Instabilities in Topology Optimization: A Survey on Procedures Dealing with Checkerboards, Mesh-Dependencies and Local Minima." *Structural Optimization* 16 (1): 68–75. https://doi.org/10.1007/BF01214002.

Sigmund, Ole. 1994. "Design of Material Structures Using Topology Optimization."

Sigmund, Ole, Niels Aage, and Erik Andreassen. 2016. "On the (Non-)Optimality of Michell Structures." *Structural and Multidisciplinary Optimization* 54 (2): 361–73. https://doi.org/10.1007/s00158-016-1420-7.

Stromberg, Lauren L., Alessandro Beghini, William F. Baker, and Glaucio H. Paulino. 2011. "Application of Layout and Topology Optimization Using Pattern Gradation for the Conceptual Design of Buildings." *Structural and Multidisciplinary Optimization* 43 (2): 165–80. https://doi.org/10.1007/s00158-010-0563-1.

Volkswagen Group. 2018. *Testing the World's First 3D Printed Brake Caliper.* https://www.youtube.com/watch?v=hPkY8nBWxoU.

Zhu, Ji-Hong, Wei-Hong Zhang, and Liang Xia. 2016. "Topology Optimization in Aircraft and Aerospace Structures Design." *Archives of Computational Methods in Engineering* 23 (4): 595–622. https://doi.org/10.1007/s11831-015-9151-2.